Forward Modeling of Post-Jurassic Shortening in the Southeast Pamir Mountains, Tajikistan

---

A Thesis Presented to

the Faculty of the Department of Earth and

Atmospheric Sciences

University of Houston

In Partial Fulfillment

of the Requirements for the Degree

Master of Science

By

Eric M Bunge

August, 2014

Forward Modeling of Post-Jurassic Shortening in the Southeast Pamir Mountains, Tajikistan

Eric M Bunge

APPROVED:

Dr. Alexander Robinson, Advisor

Dr. Michael Murphy

Dr. Jerome Guynn
ExxonMobil Corporation, Houston, Texas

Dean, College of Natural Sciences and Mathematics

Acknowledgements

My special thanks to Dr. Alex Robinson for his guidance and inspiration. It has been a pleasure working with such a knowledgeable, regional expert. Thanks also to Dr. Michael Murphy for his consultation and technical feedback and to Dr. Jerome Guynn for the nights and pints he sacrificed to encourage this project. My most sincere gratitude to my wife, Lora Bunge. Without her support and sacrifice, there is no way this project would have ever come to completion. I would also like to thank my parents, Jim and Nadene Bunge, and my wife's parents, Steve and LaVonne Oenning, for their support and encouragement over the years. I am also grateful to Svetlana Borodina and Jeff Whitehurst for their help in selected translation of the old Soviet maps. The Soviet maps served as the backbone for this project.

Forward Modeling of Post-Jurassic Shortening in the Southeast Pamir Mountains, Tajikistan

---

An Abstract of a Thesis Presented to

the Faculty of the Department of Earth and Atmospheric Sciences

University of Houston

In Partial Fulfillment

of the Requirements for the Degree

Master of Science

By

Eric M Bunge

August, 2014

Abstract

One outstanding issue in understanding the Cenozoic evolution of the Himalayan-Tibetan orogen is determining variations in the amount of crustal shortening along the length of the orogen. Current estimates assign ~50%-80% more Cenozoic intra-Asia shortening to the western portion as compared to the central and eastern portions of the orogen, while the eastern portion has accommodated ~25% more convergence overall. These estimates for the western end of the orogen rely on old compilations of shortening, which have since been recognized to have significant flaws, requiring re-evaluation to better understand the nature of along strike variation. Cenozoic internal shortening in the South Pamir has been estimated to be ~240 km. However, ~110 km of this was attributed to a nappe structure that has since been reinterpreted as an extensional detachment fault related to exhumation of the Shakhdara and Alichur gneiss domes.

In this study, I forward model the deformation in Jurassic marine carbonates of the fold and thrust region of the Southeast Pamir. This model constrains the magnitude of post-Jurassic deformation in this area in order to re-evaluate the previous estimate of 50km of Cenozoic shortening. In order to recreate the interpreted surface structures, my forward modeling suggests: 1) A dual vergent system, with northeast-directed structures in the south- and southwest-directed structures in the north. 2) Three main detachment levels; A) lower levels including basement involved thrusting and at the base of the Permian to Triassic section, B) a detachment in the upper Permian to Triassic section, and C) a detachment at the base of the Jurassic section on the lower Jurassic unconformity. 3) The detachments in the Permian to Triassic section suggests reactivation of structures formed during pre-Jurassic deformation.

My forward model yields 7.5 km of northeast-southwest shortening across the Southeast Pamir, significantly less than the previous estimate of 50 km. This reduces the previous estimate of ~240 km of internal shortening in the Southern Pamir to ~90 km. These results suggest that the magnitude of Asian internal shortening is more consistent along the strike of the orogen than previously recognized. This revised shortening estimate also requires crustal underthrusting of the Pamir in order to account for the current crustal thickness.

Contents

List of Abbreviations

P: Permian

Tr: Triassic

P-Tr: Permian to Triassic

Jr: Jurassic

GIS: Geographic Information System

DEM: Digital Elevation Model

RPZ: Rushan Pshart Zone

SE Pamir: Southeast Pamir

S Pamir: South Pamir

1. Introduction

The Pamir Mountains lie at the western end of the Himalayan-Tibetan orogeny (Figure 1) and consist of a northward-directed salient which deflects the largely east-west-trending microcontinents and magmatic belts that make up the larger Himalayan-Tibetan Orogeny (Figure 2) (Tapponnier et al., 1981; Burtman and Molnar, 1993; Schwab et al., 2004; Robinson et al., 2012). Accretion of Gondwanan terranes along the southern boundary of Asia occurred during the Paleozoic to Mesozoic in a series of, what are considered to be, 'soft-collisions' that did not result in significant continental thickening in the region (Murphy et al., 1997; van Hinsbergen et al., 2012). In the Pamir, the Cenozoic collision between India and the southern boundary of Asia is generally interpreted to have resulted in most of the regional crustal thickening and structural shortening (Burtman and Molnar, 1993; Schwab et al., 2004; Robinson et al., 2012; van Hinsbergen et al., 2012). This is in contrast with Tibet, where much of the crustal shortening and thickening is interpreted to pre-date the Cenozoic, during the development of an Andean plate boundary along the southern margin of Asia (Murphy et al., 1997; Kapp et al., 2005; Kapp et al., 2007; Leier et al., 2007).

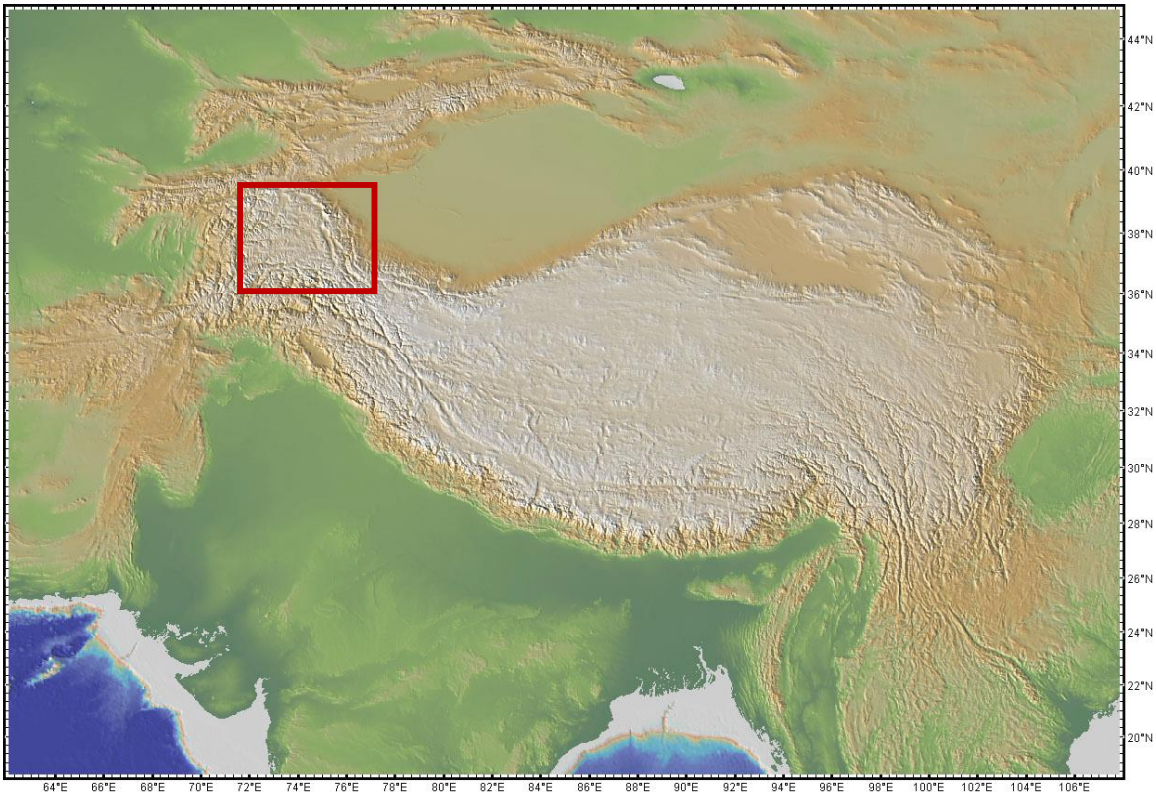

Figure 1: DEM of the Himalayan-Tibetan orogen with the location of the Pamir.

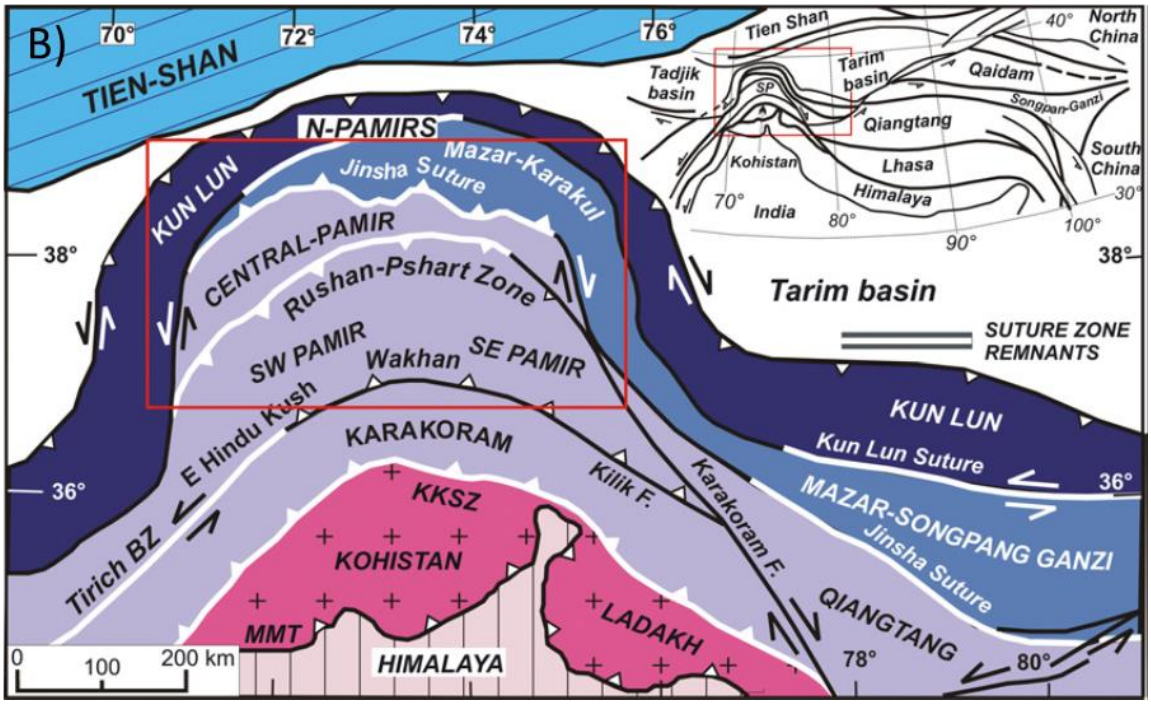

Figure 2: Simplified tectonic map of the Pamir displaying the general tectonic terranes, major faults, and sutures (Angiolini et al., 2013).

To better describe the total magnitude of India-Asia convergence, the shortening has been assigned to categories based on terrains and mechanisms. Recent studies have suggested that significantly more (50%-80%) Cenozoic intra-Asia shortening has occurred in the western portion (~ 1,200 km) of the Himalayan-Tibetan orogen, as compared to the central (~800 km) and eastern portions (~660 km) (Figure 3) (van Hinsbergen et al., 2012). This larger intra-Asia Cenozoic convergence in the Pamir-Karakoram region includes Cenozoic shortening estimates in the Pamir compiled by Burtman and Molnar (1993) which total ~655 km, including ~315 km of overthrusting of the Pamir salient over the Tajik-Tarim basins, and ~340 km of internal shortening. However, the calculated internal shortening values include over 110 km of shortening attributed to an interpreted thrust nappe in the SE Pamir (Burtman and Molnar, 1993), which has since been recognized to be a low angle extensional faults associated with gneiss dome extrusion (Stübner et al., 2013). This new interpretation removes 110 km of shortening from the compiled estimates and suggests the need to revisit previous interpretations of internal shortening values in the Pamir. Thus, it may be that the magnitude of Asian internal shortening is more consistent along the strike of the orogen than previously recognized.

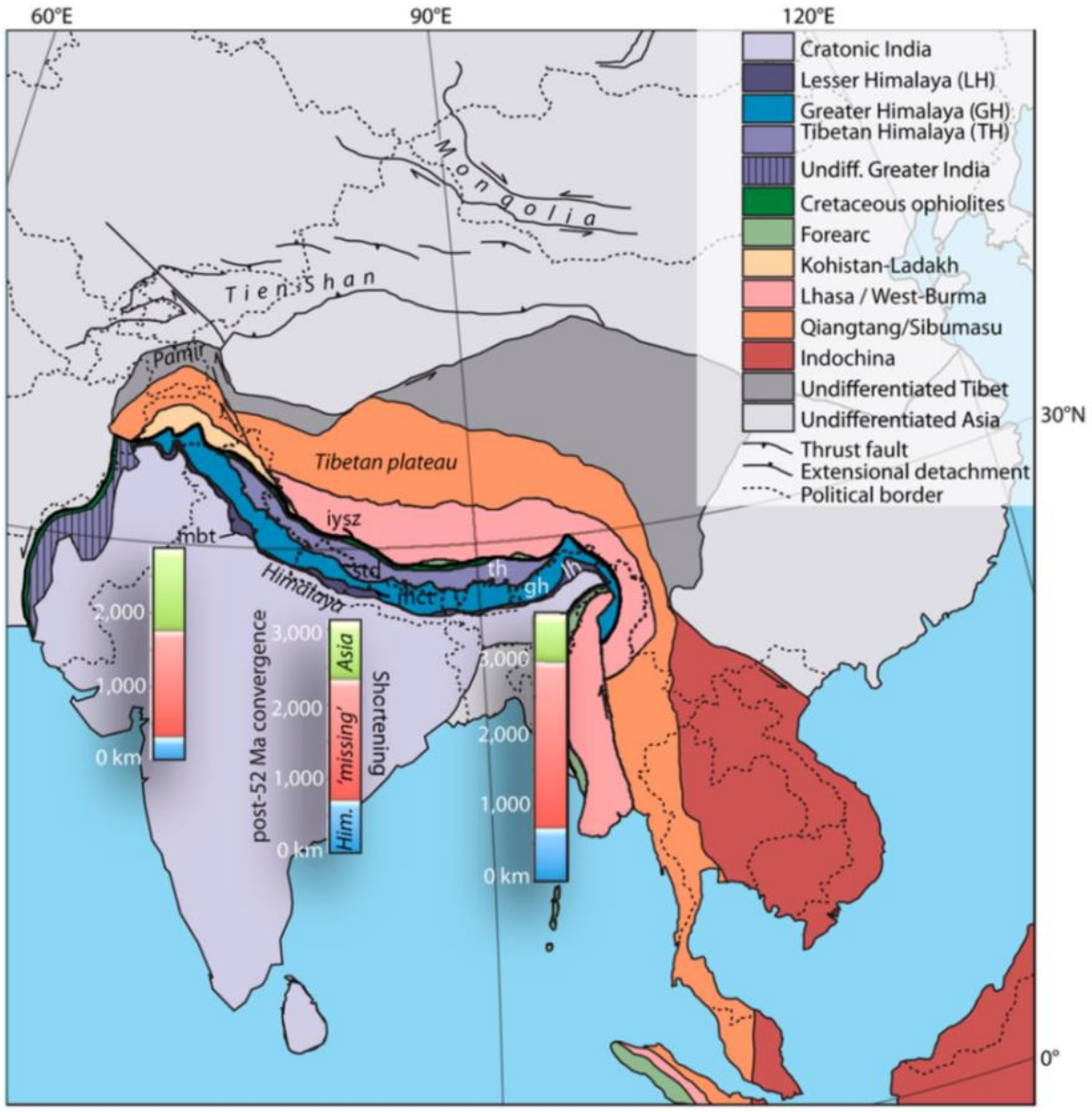

Figure 3: Total amount of convergence attributed to different portions on the India – Asia Collision zone. The green portion of the bar accounts for intra-Asia collision, the red portion represents 'missing' shortening, and the blue portion is Himalayan shortening. (van Hinsbergen et al., 2012).

The SE Pamir consists of a polyphase fold and thrust system recording a late Triassic deformation episode attributed to collision between the Central and Southern Pamir terranes, and post-Jurassic shortening generally attributed to the Cenozoic India-Asia collision (van Hinsbergen et al., 2012; Angiolini et al., 2013). Jurassic marine carbonates were deposited above the late Triassic angular unconformity and serve as an important

strain marker to record the post-early Jurassic shortening (Angiolini et al., 2013), which has previously been interpreted to be ~50 km (Burtman and Molnar, 1993). My study uses this Jurassic carbonate to construct a forward modeled cross section and finds internal shortening of the SE Pamir to be~7.5 km, significantly less than the previous interpretation.

2. Regional Geologic Setting

2.1. Pamir Overview

The Pamir-Karakoram region is marked by a pronounced northward deflection in the western portion of the east to west trending tectonic terranes of the Himalayan-Tibetan orogen which resulted from the collision between Asia and Gondwanan affinity terranes during the Mesozoic and the subsequent collision with the Indian plate during the Cenozoic (Figure 1) (Tapponnier et al., 1981; Yin and Harrison, 2000; Schwab et al., 2004). The Pamir, along with the larger Himalayan-Tibetan orogen, is made of up of a series of tectonic belts formed by suture bound microcontinents and magmatic arcs (Figure 2) (Tapponnier et al., 1981; Burtman and Molnar, 1993; Schwab et al., 2004; Robinson et al., 2012).These tectonic belts record a complex pre-Cenozoic history of basin evolution and continental accretion of distinct Gondwanan terranes onto the southern margin of Asia during the Late Paleozoic to Mesozoic, prior to Cenozoic collision of the Indian continent with Eurasia (Robinson et al., 2012; Angiolini et al., 2013). The prolonged history of terrene accretion and orogenesis has resulted in a complex setting of suture belts and interleaving tectonic terranes (Angiolini et al., 2013).

2.2. Tectonic Terranes of the Pamir

The Pamir Karakoram region has been divided into four suture-bound terranes (Figure 2): The Northern Pamir is the southern margin of Eurasia and is bound by the Main Pamir Thrust to the north and the Tanymas in the south; the Central Pamir, of Gondwanan affinity, extends from the Tanymas Suture to the Rushan-Pshart zone to the south; the Southern Pamir-Karakoram, of Gondwanan affinity, continues to the south to the Shyok suture (Robinson et al., 2012) ; and the Kohistan-Ladakh island arc terrane which continues southward to the Indus Suture (Robinson et al., 2012). Some authors have noted the occurrence of a possible suture zone along the Tirich Mir Fault, that may separate the Southern Pamir and Karakoram (Zanchi et al., 2000; Angiolini et al., 2013)

2.2.1. Northern Pamir

The Northern Pamir represents the Paleozoic-Triassic southern margin of Asia. It is a composite terrane consisting of two distinct terranes: 1) The western portion consists of the continuation of the Paleozoic North and South Kunlun terranes of western Tibet. 2) The eastern portion is dominated by Permian-Triassic granitoids and metasediments of the Karakul-Mazar terrane. The Karakul-Mazar terrane developed as an accretionary prism during the northward subduction of the Paleo-Tethys Ocean and is considered equivalent to the Songpan-Ganzi terrane of the Himalaya (Schwab et al., 2004; Robinson et al., 2012). The southern margin of the Northern Pamir is the Late Triassic-Early Jurassic Tanymas suture which marks the boundary between Eurasian crustal fragment and Gondwana crustal fragments (Central and Southern Pamir) (Robinson et al., 2012).

2.2.2. Central Pamir

The Central Pamir is a Gondwanan crustal fragment and is interpreted to be equivalent to the Gondwanan Qiangtang terrane of northern Tibet (Robinson et al., 2012). The Central Pamir collided with the Northern Pamir during the Early Jurassic closing of the Paleo-Tethys Ocean. This terrane contains deformed Paleozoic and Triassic-Jurassic metasiliciclatic and carbonate platform rocks. The Upper Carboniferous and Lower Permian sandstone, limestone, and marl unconformably cover Lower Paleozoic shale and carbonates. (Schwab et al., 2004). Basement outcrops occur in the Muskol and Sares Antiforms which are intruded by small bodies of metagabbro and diorite. The Muskol and Sares domes consist of biotite gneiss, and kyanite-bearing garnet-mica schist with Paleozoic protolith ages (Schwab et al., 2004)

2.2.3. Southern Pamir

The Southern Pamir-Karakoram terrane broke away from Gondwana in the Early Permian and has also been correlated to the Qiangtang terrane based on a limited amount of slip on the Karakoram fault (Robinson, 2009). The Central and Southern Pamir were separated by a small ocean basin, the Rushan-Shuanghu Basin. The Rushan-Shuanghu basin was closed at the end of the Triassic and the Central and Southern Pamir collided with Eurasia during the early Cimmerian orogeny (Burtman and Molnar, 1993; Angiolini et al., 2013). The Southern Pamir may be separated from the Karakoram by a suture zone along the Tirich Mir fault which is also interpreted to have closed in the Late Triassic-Early Jurassic (Zanchi et al., 2000; Zanchi and Gaetani, 2011; Angiolini et al., 2013).

The South Pamir can be divided into two regions, the Southeast and Southwest Pamir (SW Pamir), which are separated by Cenozoic extensional detachment faults that

developed on the flanks of large gneiss domes. The SW Pamir gneiss domes consist of Precambrian age rocks with Oligocene-Miocene metamorphic peak ages (Angiolini et al., 2013; Stübner et al., 2013). These domes are interpreted to represent the crystalline basement underlying the entire southern Pamir. The SE Pamir consists of a well preserved Late Paleozoic to Mesozoic sedimentary section above the crystalline basement.

2.3. Tectonostratigraphy of SE Pamir

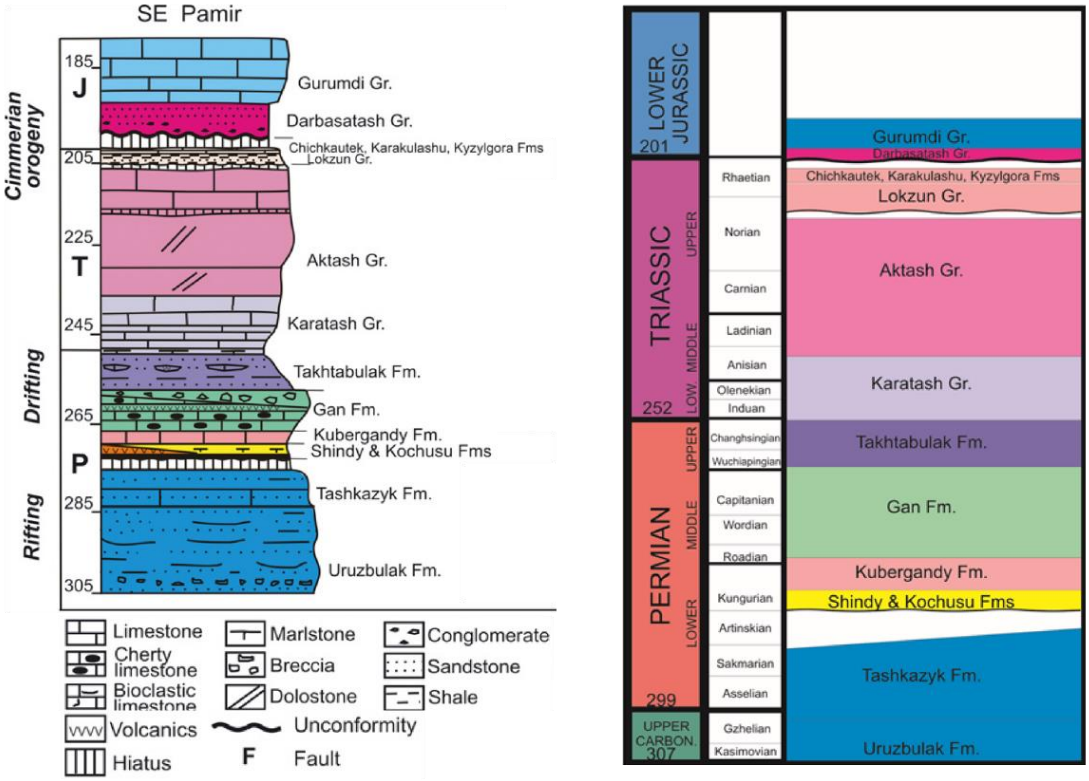

Figure 4: Synthetic chrono-stratigraphic section of the Southeast Pamir (Angiolini et al., 2013)

The stratigraphy of the SE Pamir records rifting from Gondwana in the late Paleozoic, drifting during the Late Permian through Triassic, and collision with Asia in the latest Triassic-earliest Jurassic. Collision was accompanied by shortening followed by a period of erosion, and then subsequent marine carbonate platform development in the Jurassic.

This was followed by another phase of shortening in the Cenozoic. The base of the section which records the rifting phase are the siliciclastics of the Uruzbulak and Tshkazyk Formation (Upper Carboniferous-Lower Permian) (Figure 4). These sediments vary in thickness throughout the region and are overlain by a middle upper Permian carbonate platform. The Permian carbonate is capped by an unconformity interpreted to mark the transition to the drifting phase (Angiolini et al., 2013). This transition is also marked by the inter fingering of slope and basinal facies of the Kochusu, Shindy, Kubergrandy, Gan, and Takhtabulak formations which are comprised of bioclastic limestones, cherty limestones, shales, volcaniclastics, sandstone, and conglomerates with debris flow deposits and olistostromes (Angiolini et al., 2013).

The Triassic section includes the Karatash and Aktash Group carbonate platform sediments overlain by the Lokzun Group Rhaetian flysches (Figure 4). The Upper Triassic section has been interpreted to record the closure of the Rushan Shuanghu Basin. (Angiolini et al., 2013).

The Permian-Triassic succession is capped by a spectacular angular unconformity (Figure 4) marking the end of one phase of shortening. This unconformity truncates the highly deformed Permian to Triassic section and is overlain by the lowermost Jurassic Darbasatash group, a gently dipping sequence of interbedded red conglomerate and sandstone that is conformably overlain by the Hettangian Limestones of the Gurumdi Group. These lower Jurassic sedimentary rocks are marine showing that the terrane had fallen below sea level. The Jurassic section is deformed by NW-SE-trending folds and thrust faults which contrasts with the fold orientation of the underlying Triassic succession in places (Angiolini et al., 2013).

The angular unconformity at the base of the Jurassic section separates two phases of shortening based on different trends of the structures. The Triassic shortening event is interpreted to be the results of the closure of the Rushan Shuanghu Basin. This event is interpreted to be a soft collision with limited crustal thickening as the Southern Pamir was lowered to below sea level by the Early Jurassic to create the angular unconformity and deposit the Jurassic marine strata (Angiolini et al., 2013).

2.4. Previous Estimates of Crustal Shortening in the Pamir

The total amount of convergence between the Indian and Asian plates is well constrained using tectonic plate circuits based on oceanic ridge spreading and paleomagnetic data (Le Pichon et al., 1992; van Hinsbergen et al., 2012). Since initial collision at 52 Ma (Zhu et al., 2005), the two plates have converged a total of 3,600 ± 35km. This varies along the length of the orogen with more convergence in the eastern Himalaya and less in the Pamir-Karakoram area (Figure 3). This convergence is categorized as: 1) shortening within the Asian Plate, 2) shortening within the Indian Plate, and 3) "Missing shortening" (generally attributed to subduction or lateral extrusion) (van Hinsbergen et al., 2012).

Regional compilations suggest the western portion of the India-Asia collision zone (including the Pamir) has accommodated much more shortening within the Asian Plate (~ 1200 km) than the Central (~800 km) and Eastern (~660 km) Tibetan Plateau (van Hinsbergen et al., 2012). These values are from first-order estimates of magnitudes and mechanisms of shortening across the orogen, some of which have since been reinterpreted and need revision based on more recent and rigorous studies.

A large portion of Cenozoic intra-Asian convergence in the western portion of the orogen has been attributed to the Pamir where Burtman and Molnar (1993) interpreted there to be ~655 km of Cenozoic shortening. They attribute ~315 km of this convergence to thrusting of the Pamir salient over the Tajik-Tarim basin as seen in the northward arcuate deflection of the tectonic terranes around the Pamir, paleomagnetic anomaly restoration, facies terminations, and the southward subducted continental lithosphere here (Burtman and Molnar, 1993; Thomas et al., 1994). Another ~340 km of shortening is taken up by Cenozoic internal shortening of the Pamir with 240 km in the Southern Pamir and 100 km in the Central Pamir (Burtman and Molnar, 1993).

In the Central Pamir, Burtman and Molnar (1993) attributed most of the Cenozoic shortening to the emplacement of the Vanch, Akbaital, and Zortashkol nappes (Figure 5). In this interpretation, the Central Pamir is over-thrust by the Northern Pamir by about 80 km. Folding within the hanging wall and footwall of these structures is estimated to add another 20 km of shortening to the Central Pamir for a total of 100 km of Cenozoic shortening (Burtman and Molnar, 1993).

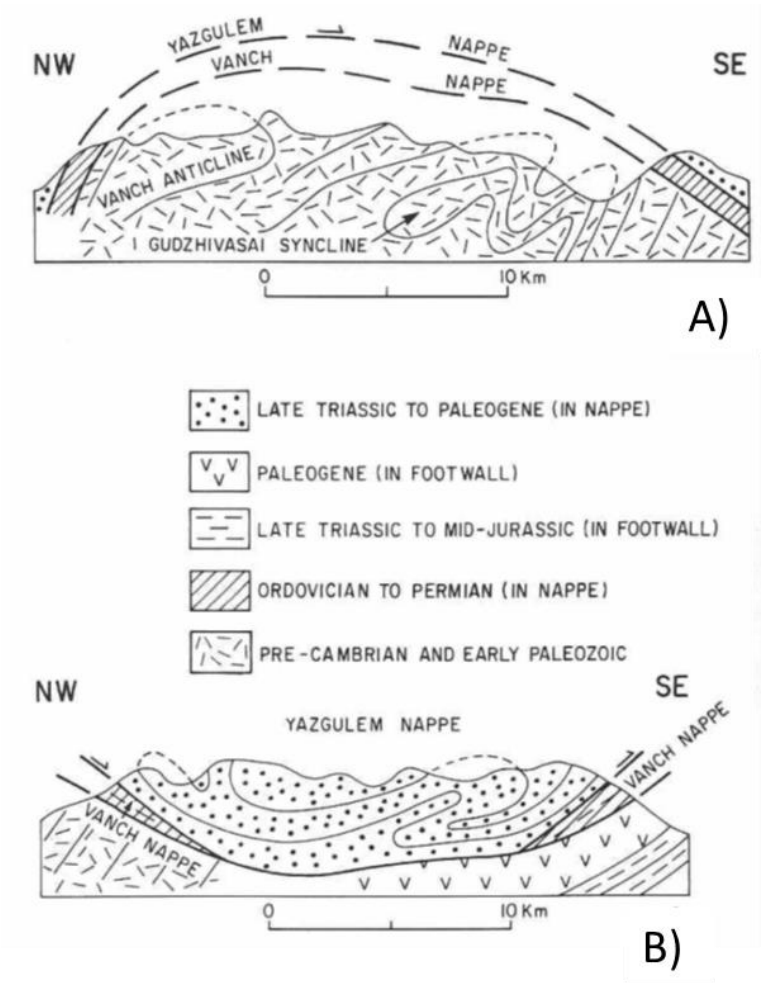

Figure 5: Yazgulem and Vanch nappes in Central Pamir. Note overturned and recumbent folds (Burtman and Molnar, 1993). Location shown in Figure 6B

Within the Southern Pamir, a magnitude of 240 km of shortening was estimated with the largest portion (minimum 110 km) attributed to the emplacement of a nappe. This interpretation noted the tectonic contact between basement and sedimentary rock and interpreted it as a nappe thrust (Figure 6). This decollement has since been recognized to be a low-angle normal fault associated with the exhumation of Cenozoic Shakhdara and Alichur gneiss domes (Figure 7) (Stübner et al., 2013). This new interpretation removes a minimum of 110 km from the magnitude of Cenozoic internal shortening, reducing the estimate for the Southern Pamir to ~130 km.

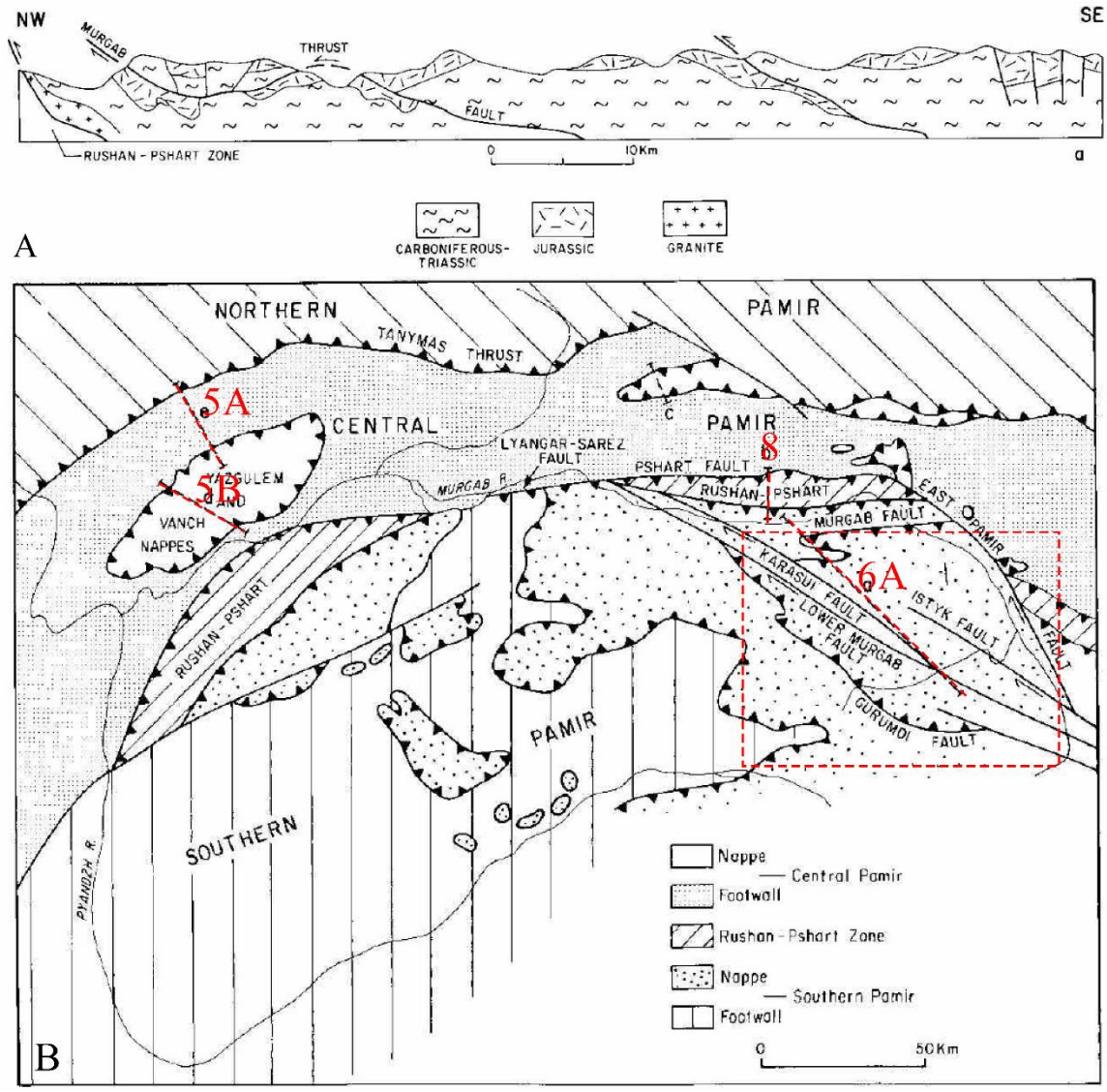

Figure 6: A) Cross section showing thrusted nappe structures across the Murgab Fault. Location is shown in Figure 6B (Burtman and Molnar, 1993) B) Simplified Geologic Map showing the Thrust nappe Interpretation, cross section locations, and the area of interest of this study (Burtman and Molnar, 1993).

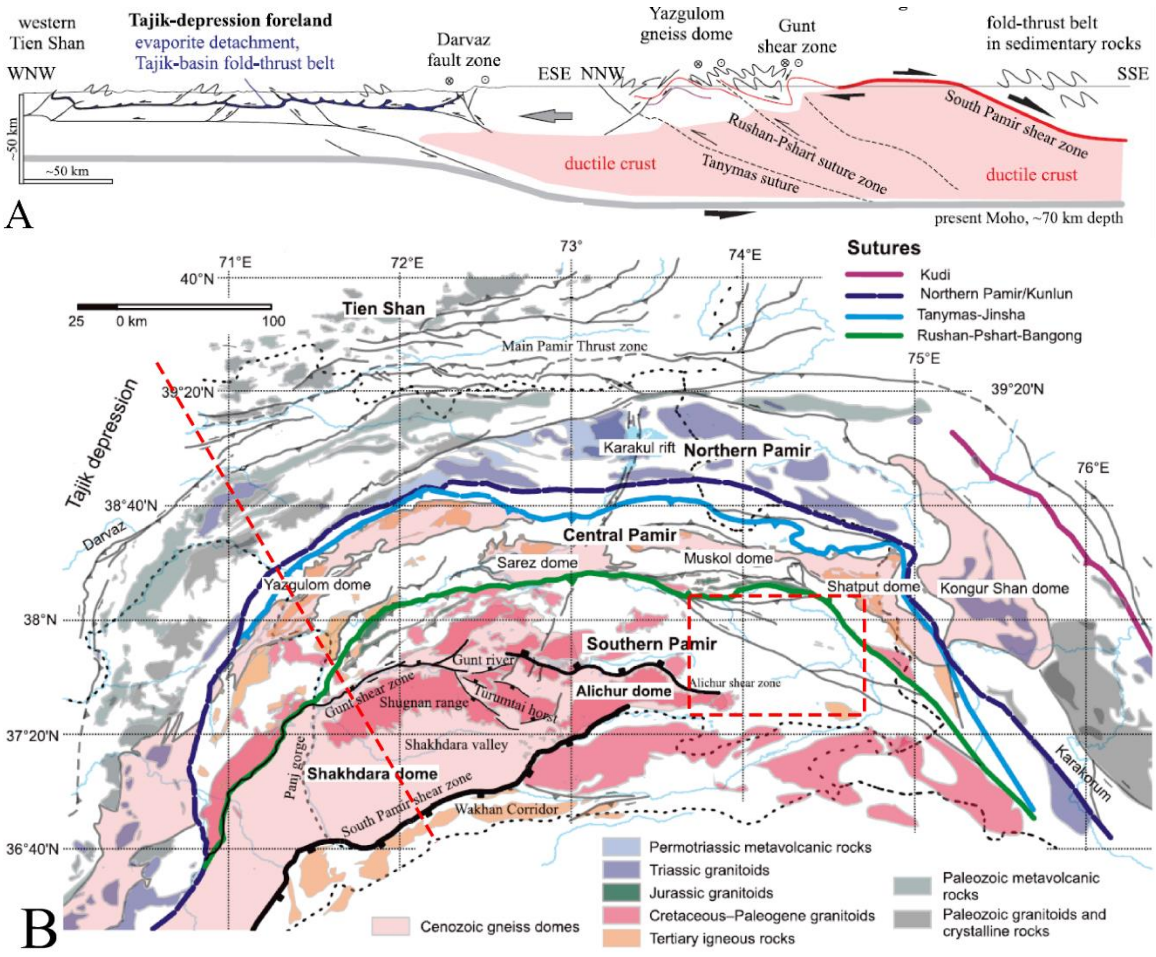

Figure 7: A) Cross section depicting the vertical extrusion of the Shakhdara dome, linked thrusting to the north in the Rushan-Pshart zone, Tanymas Suture and out into the Tajik-depression foreland with estimated deep detachment at the Moho (Stübner et al., 2013) B) Geologic map of the Pamir noting the low angle normal faults linked to the thrust / suture faults , a cross section location, and the area of interest for this study (Stübner et al., 2013).

The remaining shortening in the Southern Pamir is attributed to: 1) 50 km of shortening within the fold and thrust belt of the SE Pamir and movement along the Murgab and Gurumdi faults in the fold and thrust belt of the SW Pamir; and 2) 80 km of shortening to the cumulative movement along the NW trending right lateral strike-slip faults of the Aksu-Murgrab (50 km) and East Pamir Fault systems (30km) (Burtman and Molnar, 1993). This strike slip displacement was absorbed by north-directed-

thrusting/underthrusting on the Pshart and Lyangar-Sarez faults (Figure 8) which moved the Rushan-Pshart over the Central Pamir, (Burtman and Molnar, 1993).

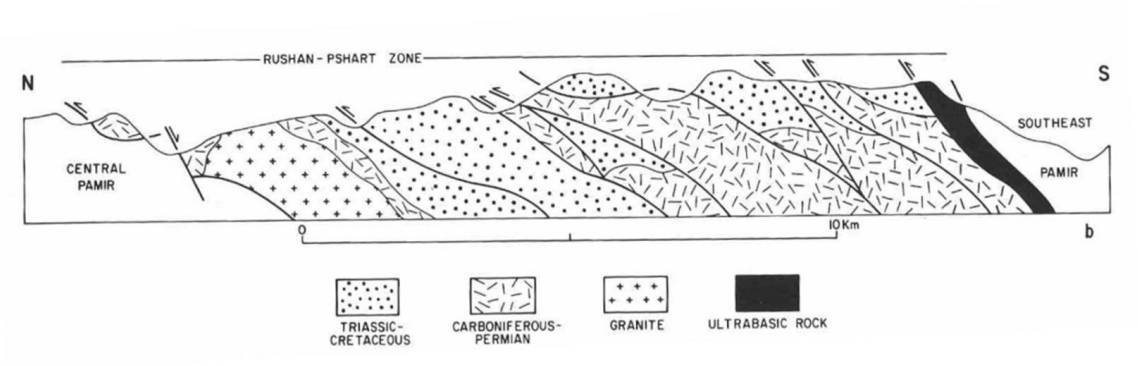

Figure 8: Imbricate thrusting within the Rushan-Pshart zone and over-thrusting on the Central Pamir and under-thrusting under the Southern Pamir (Burtman and Molnar, 1993). Location shown in Figure 6B.

The cumulative shortening within the South Pamir as summarized above was also compared to slip along the larger Karakoram strike slip fault which cuts across the region. Burtman and Molnar noted 340 km of displacement along the Karakoram fault, roughly agreeing with uncorrected S Pamir shortening estimate of ~240km. However, Robinson (2009) documented only 149-167 km of right lateral separation along the Karakoram fault (Robinson, 2009) which agrees with the corrected Cenozoic shortening estimate of ~150 km for the S Pamir (Burtman and Molnar, 1993; Stübner et al., 2013).

To summarize, Burtman and Molnar (1993) attributed ~655 km of Cenozoic shortening/displacement to the Pamir. Approximately 340 km of this was attributed to internal shortening within the Northern to Southern Pamir with ~240 km assigned to the internal shortening of the Southern Pamir and the Rushan-Pshart Zone. However, the recognition that ~110 km of this was based on misinterpretations of regional structures warrants the need to re-evaluate the shortening on other regional structures. This study examines the magnitude of post-Jurassic shortening in the SE Pamir by modeling the

deformation of a Jurassic Limestone (Figure 9) in the area to better constrain the ~50 km budget proposed by Burtman and Molnar (1993).

3. Geology of the Southeast Pamir

3.1. Area of Interest

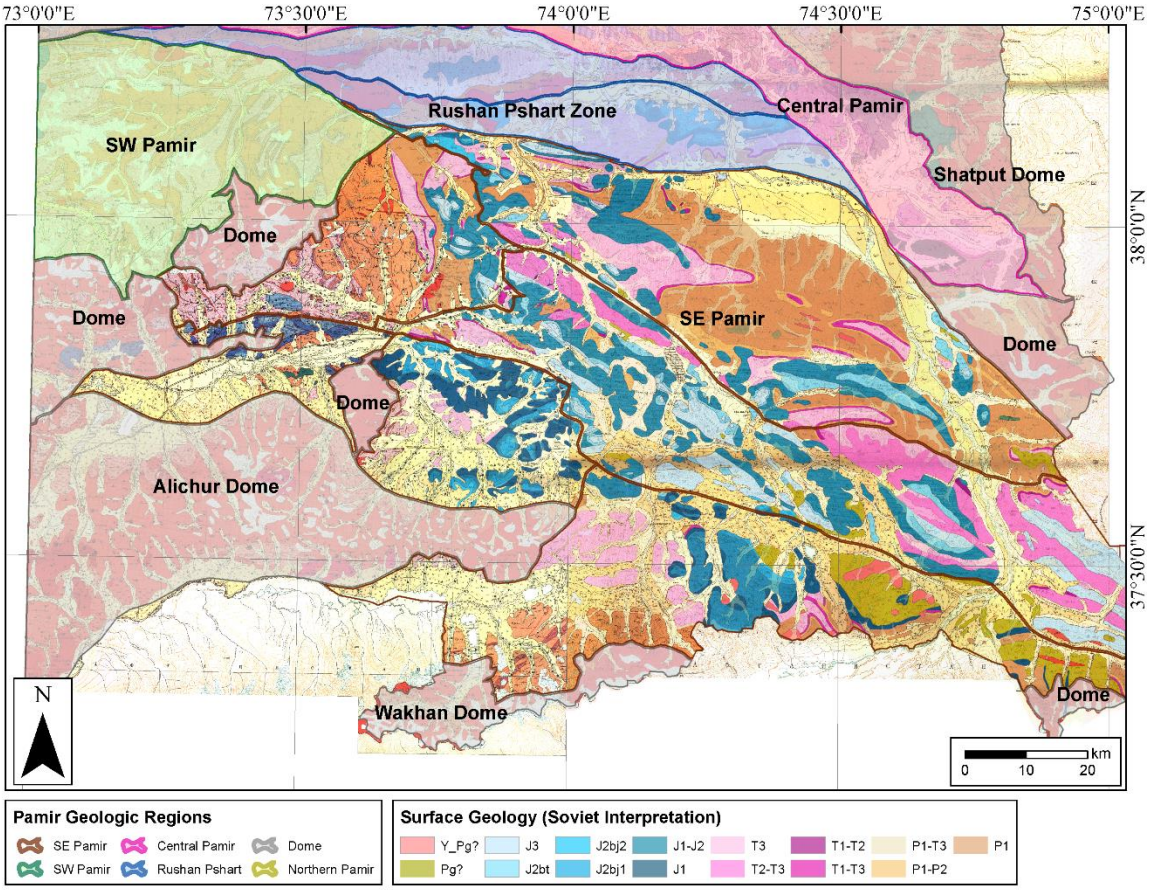

Figure 9: Map of SE Pamir and the surrounding geologic regions. The SE Pamir is unshaded and displays the surface geologic interpretation presented in the 1:200,000 Soviet Geologic Maps (Yushin et al., 1964). The surface geology of the SE Pamir is comprised primarily of the Permian through Jurassic section with Paleogene (?) and Quaternary cover. The surrounding geologic areas are color shaded and labeled.

The area of interest is within the Southeastern Pamir where the Jurassic units are well preserved (Figure 9). The area is bound to the north by the Rushan-Pshart Zone, to the south by the Alichur and Wakhan Domes, to the east by the Karakoram, and to the west

by the Southwest Pamir. Geopolitically, this area is located almost entirely within Eastern Tajikistan.

3.2. Stratigraphy of the SE Pamir

The stratigraphy of the SE Pamir is dominated by Permian to Jurassic rocks. A compilation of previously published data and a stratigraphic column from the primary 1:200,000 Soviet geologic map (Yushin et al., 1964) were used to constrain lithologies and unit thicknesses over the area of interest. At the base of the section is the Upper Carboniferous-Lower Permian succession comprised of the Uruzbulak and Tashkazyk (Pennsylvanian-Artinskian) formations of the Bazar Dara Group (Figure 4). This section has broad variations in thickness of 300-2000 m and consists of medium-grained siliciclastic and bioclastic rocks (Angiolini et al., 2013).

Middle-Upper Permian strata unconformably overlie the Bazar Dara Group and are comprised of massive bioclastic limestones of the Kurteke Formation interpreted to be platform facies (Angiolini et al., 2013). At the base of the Middle-Upper Permian is the Kochusu Formation which consists of slope to basin facies silty and marly limestones, the Shindy Formation which consists of massive trachy-basalts and pillow texture basalts with interbedded breccias and volcaniclastics, followed by the Kubergandy Formation made of bioclastic limestones, siltstones and volcaniclastics. Above this is the Gan Formation made of cherty bioclastic limestones with volcaniclastics and boulder-sized conglomerates (Figure 10). The upper most Permian strata is the Takhtabulak Formation made of volcaniclastics sandstone, shales, and conglomerates with olistolithes (Figure 4). Fossil content of the of the Middle-Upper Permian formations constraints their age to be

Kungurian-Changhsingian (Angiolini et al., 2013). The Upper Permian ranges in thickness between 150-180m (Figure 10).

The Triassic strata in the SE Pamir consists of the Induan, Norian Karatash, and Aktash Groups (Korchagin, 2008, 2009) which are mostly platform carbonates. These are overlain by Rhaetian age shales and sandstones of the Lokzun Group. The Lokzun Group is made of; 1) the Igrimjus Formation which consists of dark grey marly limestone and claystones (Norian Age), 2) the Bostanak Formation which consists of grey-green sandstones and siltstones, 3) the Djilga-Kochusui Formation which consists of black shales, sandstones, and limestone lenses (Rhaetian age), and 4) the Gudar Formation which consists of black siltstones (lower Rhaetian). The Lokzun Group is unconformably overlain by the Chichkautek, Karakulashu, and Kyzylgora formations which are middle-upper Rhaetian in age (Korchagin, 2009; Angiolini et al., 2013).

The Permian-Triassic section is heavily folded and capped by an angular unconformity. This angular unconformity is overlain by the Darbasatash Group, a 100 m-thick series of conglomeratic red beds (Dronov, 2006; Angiolini et al., 2013). These conglomerates are comprised of volcanic materials, Permian limestone, and arenaceous rock fragments (Garzanti et al., 2006; Angiolini et al., 2013). The Darbasatash Group is conformably overlain by the Lower Jurassic Gurumdi Group carbonates. The Gurumdi Group is made of two units. The lower unit is a 20-100 m thick dark bioclastic limestone with interbedded claystone (lower Hettangian). The upper unit is 100-300m thick and contains reefal limestones and corals (Dronov, 2006; Angiolini et al., 2013).

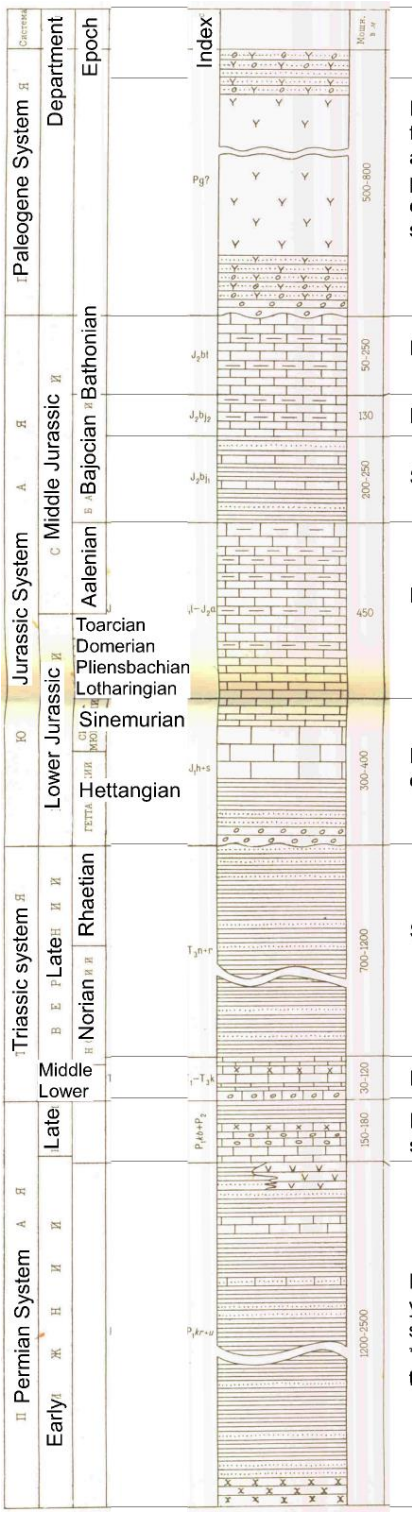

Soviet Lithology Translation	Group / Formation Equivalence form Literature
Dacite, dacito-andesites, andesite, trachyandesite, middle and acid pyroclastic and sedimentary pyroclastic rocks of acid, conglomerate, sandstone, shale, limestones	
Limestone, marlstone.	
Limestones, marlstones	
Sandstone, schist, limestones.	
Limestones, marlstones.	
Limestone, sandstone, conglomerate.	Darbasatash Gr. Darbasatash Gr.
Schist, sandstone, siltstone	Chichkautek, Karakulasha & Kyzylgora Fms. Lokzun Gr. Aktash Gr. Karatash Gr.
Limestones, siliceous schist, shale	
Limestone, siliceous schist and shale, tufa, tuff sandstone	Takhtabulak Fm.
Карачетырский* (Karachetyr) and улукские* (Uluck) floors. Schist, sandstone, effusive rocks, quartzite. *Translation is unclear, direct translation of lettering in parenthesis.	Gan Fm. Kubergandy Fm. Shindy & Kochusu Fms. Kurteke Fm. Bazar Dara Gr: Uruzbulak and Tashkazyk Fms.

Figure 10: Stratigraphic Column with translation from 1:200,000 Soviet Geologic Map, maps sheet J-43-21,22,27,28 (Yushin et al., 1964), with interpreted Group / Formation equivalence from Figure 4.

Stratigraphic and lithologic information about the middle to upper Jurassic section was constrained using the stratigraphic column from the 1:200,000 Soviet Geologic Map, map sheet J -43-21,22,27,28 (Figure 10) (Yushin et al., 1964) and observations from satellite imagery available in Google Earth. According to this information the Middle to Upper Jurassic section conformably overlies the Lower Jurassic units. The Middle to Upper Jurassic section appears to be a continuation of limestone to marlstone separated by more shale-rich units (Figure 10).

3.3. Structural Regimes in the SE Pamir

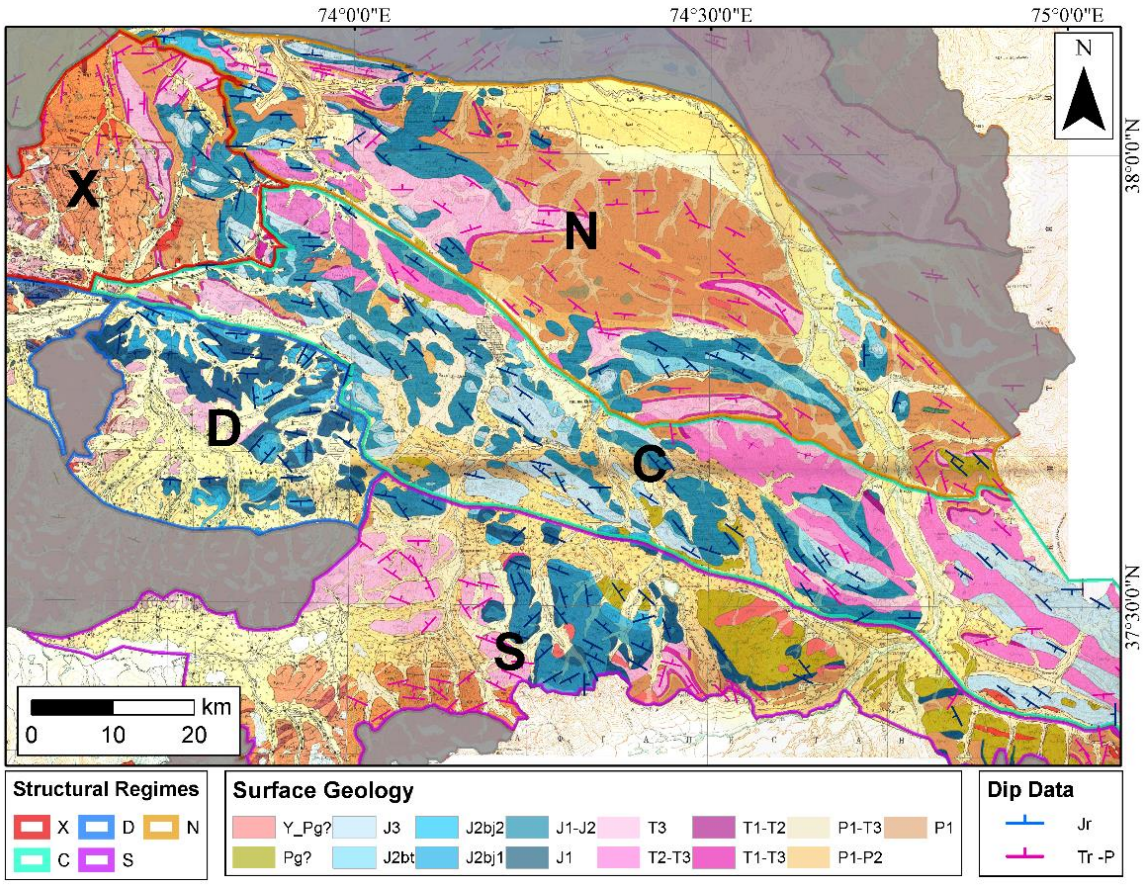

Figure 11: Map of the SE Pamir showing interpreted structural regimes based on age of rocks at surface, age above and below unconformity, structural style, and structural orientation.

In my analysis, the structures and stratigraphy as presented in the geologic maps of the SE Pamir were divided into several different structural regimes. These regimes are defined by geologic units at the surface, geologic units above and below the Early Jurassic unconformity, structural fabric, and structural orientation. The structural regimes were then used to asses and interpret stereonet analysis of the strike and dip data from the Soviet Geologic Maps and to help build the structural framework used for the forward modeled cross-section. The letters used to identify the regimes in Figure 11 are based on basic geographic relationships; 'S' for South, 'C' for Central, 'N' for North, 'D' for proximity to the Alichur Dome and 'X' for a region to the northwest which has a high angle between the Permian-Triassic and Jurassic Structural fabrics.

The maps and stereoplots (Figure 12 to Figure 15) are displayed first, followed by a detailed discussion of each regime. The stereoplots show the poles for the dip data collected from 1:200,000 Soviet Maps (Yushin et al., 1964) separated by age (Tr and older, Jr and younger) and contoured by dip density.

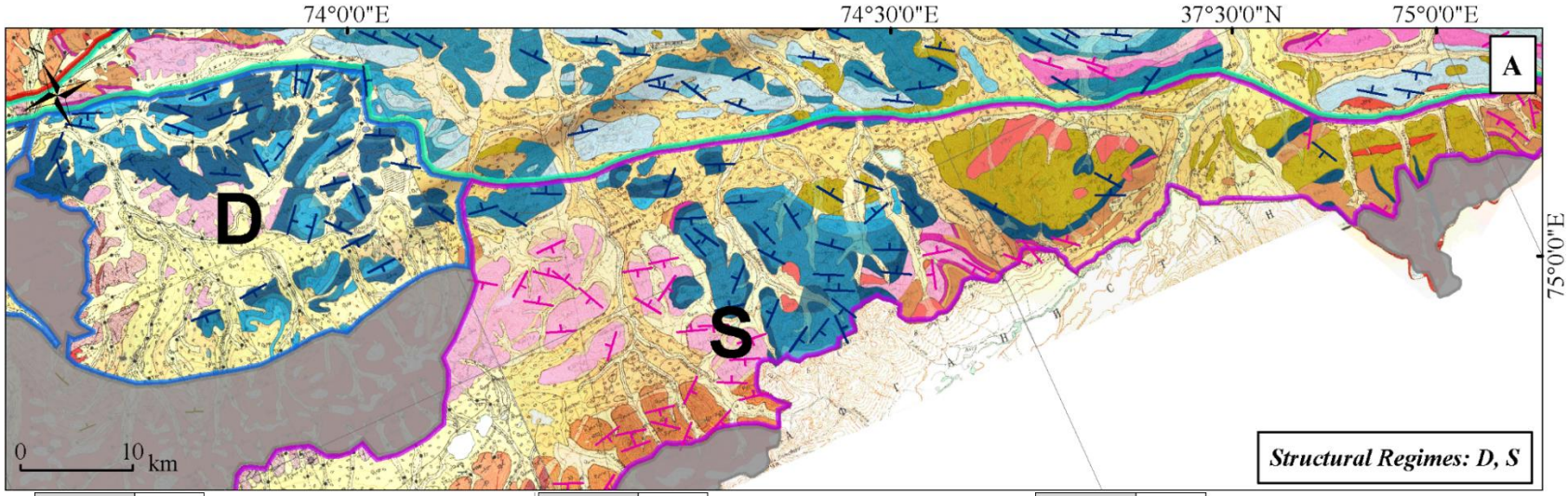

Area	S
Age	Tr
# of Points	38
SD	0.6

	Dip	Dip Az
Sec Plane	90	109.58
Mean Res Pl.	15.19	121.64
Trans. Pole	63.64	229.96
Long. Pole	14.07	109.58

B

Area	S
Age	Jr
# of Points	31
SD	0.74

	Dip	Dip Az
Sec Plane	90	116.75
Mean Res Pl.	11.9	25.09
Trans. Pole	15.72	25.86
Long. Pole	3.13	116.75

C

Area	D
Age	Jr
# of Points	34
SD	0.79

	Dip	Dip Az
Sec Plane	90	96.94
Mean Res Pl.	12.71	101.14
Trans. Pole	0.52	6.81
Long. Pole	13.75	96.94

D

Figure 12: A) Map of structural regimes D and S. Map legend same as Figure 11. The dip data are separated by age, B) Tr and older from Regime S, C) and Jr and younger from Regime S, and D) and Jr and younger from Regime D. No Tr dip data is available in Regime D.

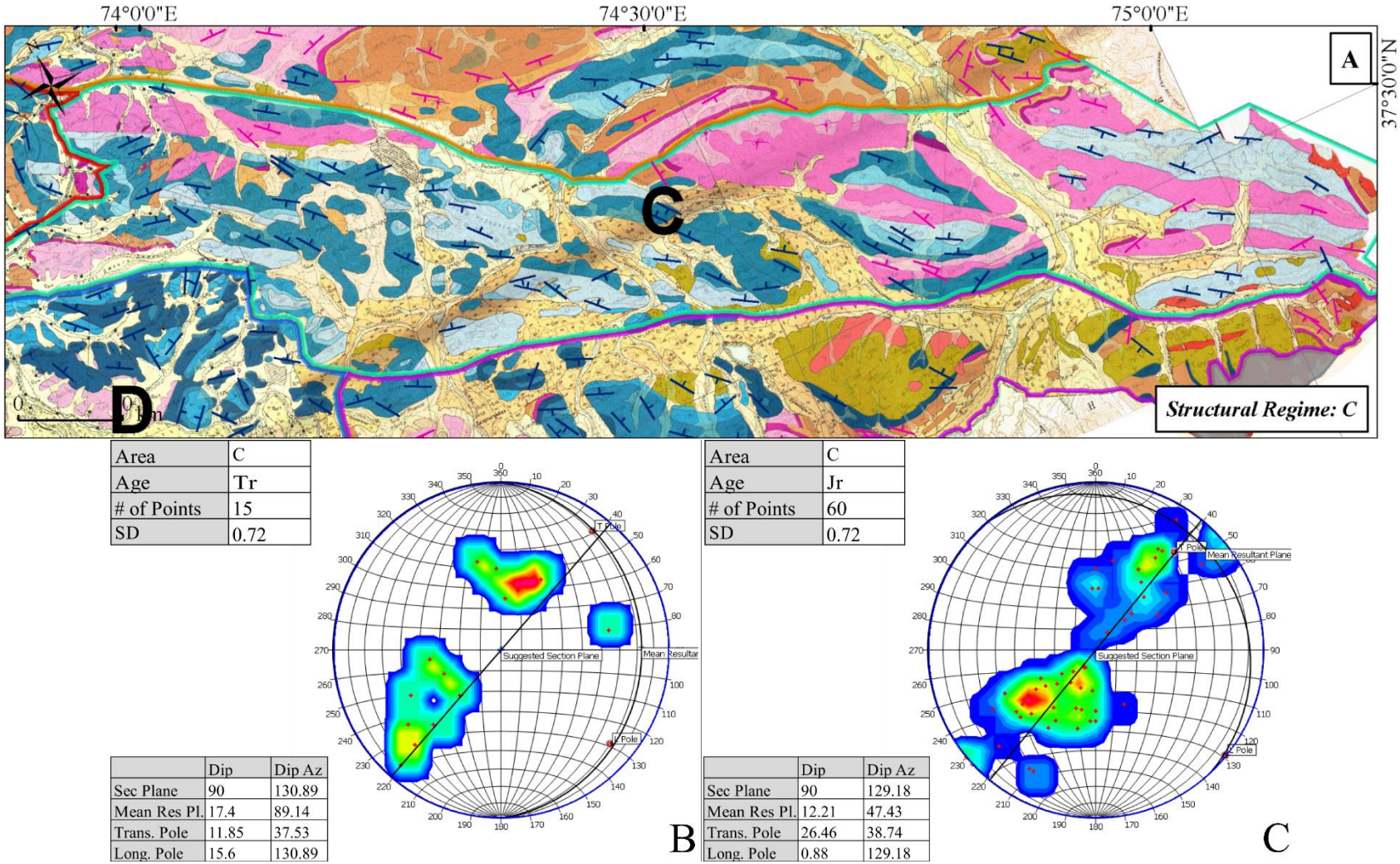

Figure 13: A) Map view of structural regime C. Map legend same as Figure 11. The dip data stereoplots are separated by age, B) Tr and older, C) Jr and younger.

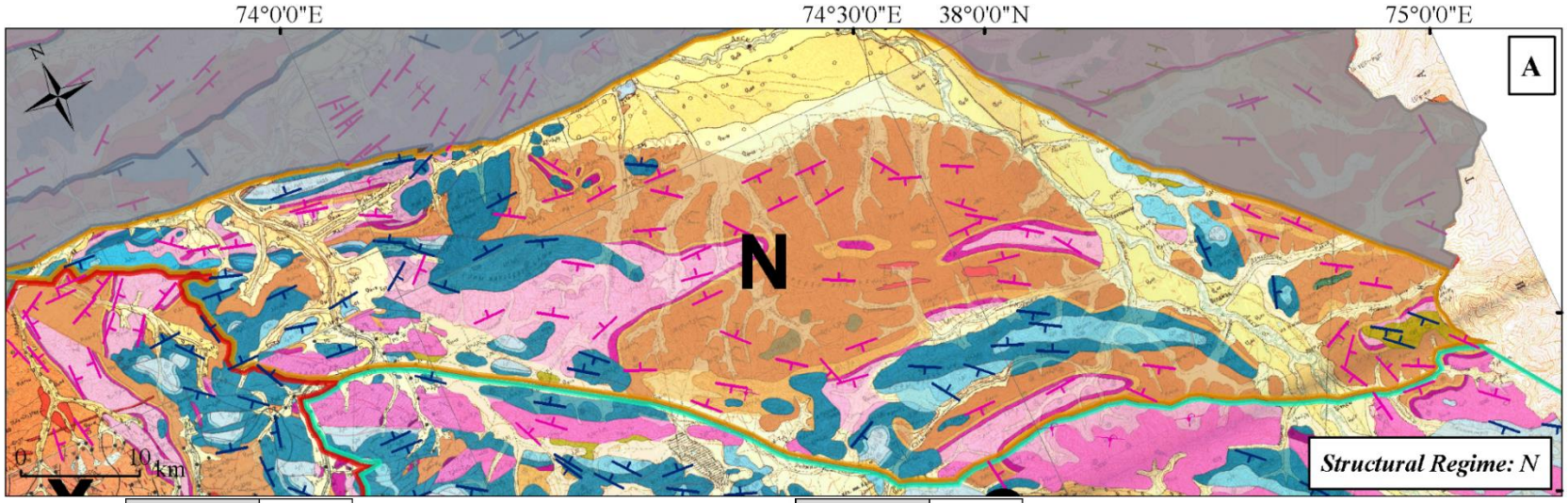

Area	N
Age	Tr
# of Points	65
SD	0.54

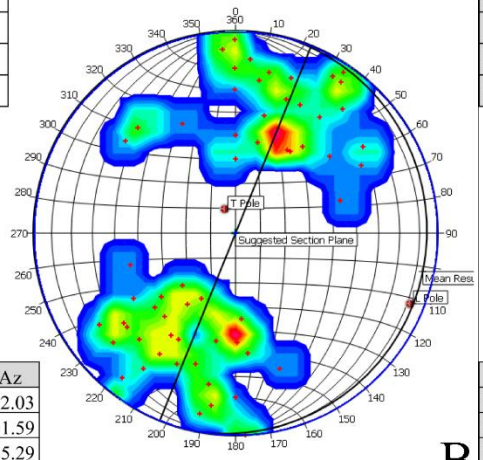

	Dip	Dip Az
Sec Plane	90	112.03
Mean Res Pl.	6.2	101.59
Trans. Pole	79.46	335.29
Long. Pole	7.71	112.03

B

Area	N
Age	Jr
# of Points	36
SD	0.73

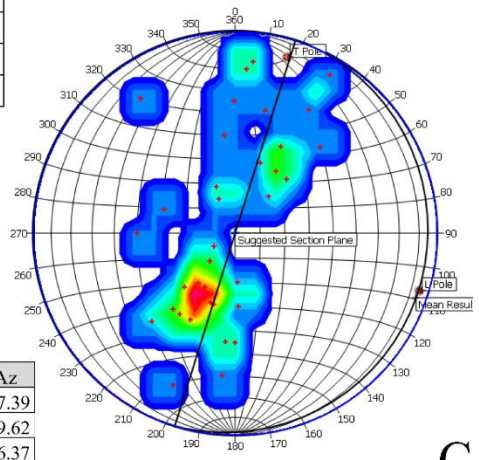

	Dip	Dip Az
Sec Plane	90	107.39
Mean Res Pl.	5.6	109.62
Trans. Pole	10.49	16.37
Long. Pole	5.48	107.39

C

Figure 14: A) Map view of structural regime N. Map legend same as Figure 11. The dip data stereoplots are separated by age, B) Tr and older, C) Jr and younger.

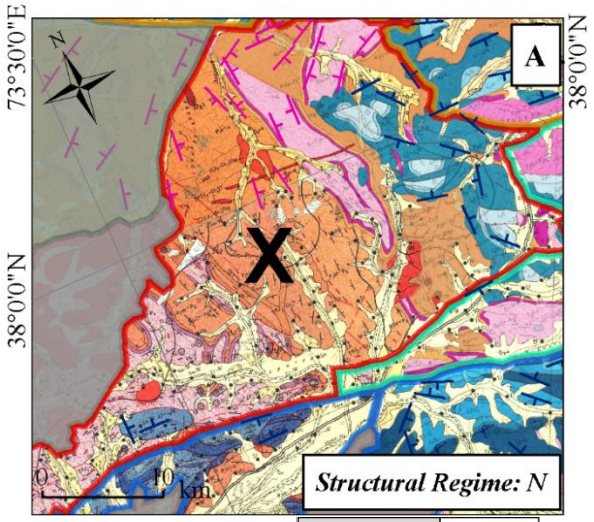

Area	X
Age	Tr
# of Points	18
SD	0.61

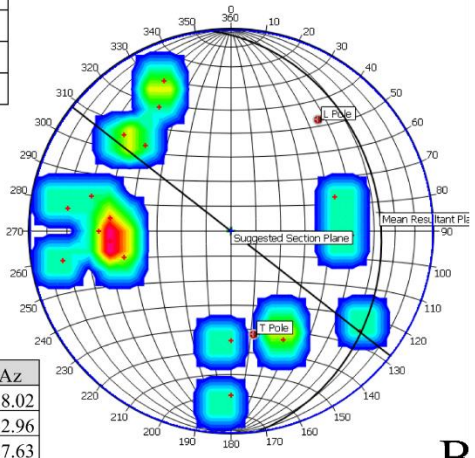

	Dip	Dip Az
Sec Plane	90	38.02
Mean Res Pl.	26.83	82.96
Trans. Pole	46.84	167.63
Long. Pole	30.88	38.02

B

Area	X
Age	Jr
# of Points	10
SD	0.74

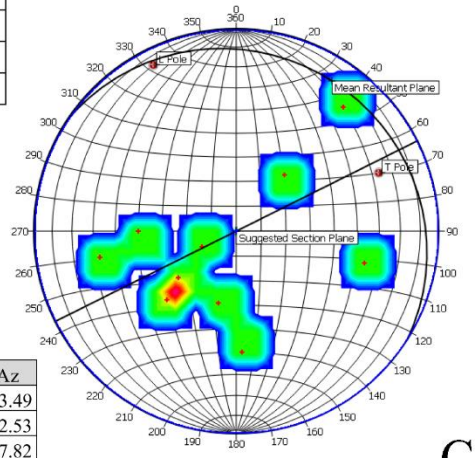

	Dip	Dip Az
Sec Plane	90	333.49
Mean Res Pl.	13.03	32.53
Trans. Pole	25.01	67.82
Long. Pole	9.18	333.49

C

Figure 15: A) Map view of structural regime N. Map legend same as Figure 11. The dip data stereoplots are separated by age, B) Tr and older, C) Jr and younger.

3.3.1. Structural Regimes D & S

The southernmost regimes of the area of interest are ‘D’ and ‘S’ (Figure 12A). Both ‘D’ and ‘S’ have the Soviet geologic unit J1 on top of the unconformity separating the Permian-Triassic and Jurassic sections. Based on the Soviet Stratigraphic Column (Figure 10), J1 is the oldest portion of the Jurassic section in this area. This geologic unit is not present in the other regimes of the SE Pamir (C, N, and X). T3 (Upper Triassic, Figure 10) also appears to be the dominant unit below the unconformity. Structures in both D and S appear to have a northeastward sense of vergence based on age juxtapositions across faults. Regimes D and S differ from one another based on the apparent structural wavelength. Regime D has a shorter structural wave length and has less Permian to Triassic section at the surface, while Regime S has a longer structural wavelength with more Triassic present at the surface. This suggests that Regime D has a shallower detachment which results in a shorter structural wavelength and brings less Permian-Triassic section to the surface. Regime S, in contrast, likely has a deeper detachment involving more of the Permian-Triassic section and as a result folds have a longer wavelength and bring up more of the Triassic section to shallower structural levels.

Dip data stereonets for Regimes D and S are separated by age; Triassic and older, and Jurassic and younger. Each of the stereonets has a solid line passing through the middle of the stereonet which is the ‘Suggested Section Plane’ provided by Midland Valley’s Move software. This best fit line is intended to fit the average dip azimuth of the data. I used this line as a proxy for the orientation of the maximum finite strain and which is also used to compare pre-and post-Jurassic deformation. In Regime S, the Suggested Section

Orientation planes are within 10° of each other suggesting that both the pre- and post-Jurassic events experienced roughly the same orientation of shortening (Figure 12B,C,D).

3.3.2. Structural Regime C

Regime 'C' is the next structural regime to the north. The lowermost Jurassic unit observed on top of the Unconformity is the Soviet Unit J1-J2 with Jurassic unit J1 not present. Deformed Permian through Triassic strata are exposed below the unconformity. The shortening direction in this region is interpreted to be south-vergent based on unit juxtapositions across faults. A portion of this section also has horizontal bedding and may be a stable structural portion in the fold and thrust belt. This largely undeformed section might be considered the regional level for the surrounding deformed units. Stereonet data indicates that the best fit plane to the dip azimuth data is within 1° between the pre-and post-Jurassic dip data, again showing the pre- and post-Jurassic shortening events in this region were similar in orientation (Figure 13).

3.3.3. Structural Regime N

Regime 'N' is the northern most regime of the SE Pamir. This section is dominated by the Permian to Triassic section which is deformed by broad folds. Above the deformed Permian-Triassic section, the Middle Jurassic (J1-J2, to J2bt) appears to be fairly flat lying above the regional unconformity. Stereonet data indicates that the best fit plane to the dip azimuth data is within 5° between the pre and post Jurassic dip data, again showing the pre- and post-Jurassic shortening events in this region were similar in orientation (Figure 14).

3.3.4. Structural Regime X

Structures in Regime ‘X’ are significantly different to the other regimes discussed above. Inspection of the geologic map (Figure 15) indicates that structures in the pre-Jurassic strata are oriented north to south while the Jurassic strata do not display consistent structural trends. Dip analysis shows that the structures in the pre-Jurassic strata dip to the northwest and southeast while the Jurassic dips are mostly northeast and southwest. The best fit planes of the dip orientations for the two age intervals are separated by over 60°. This indicates that the Pre-Jurassic deformation event involved a very different shortening direction than the Post-Jurassic deformation event or that the Pre-Jurassic structures have been rotated during the post-Jurassic deformation.

3.4 Forward Modeled Cross Section Location

The purpose of the forward modeled cross section in this study is to quantify the strain recorded by Jurassic carbonates in the SE Pamir as well as to constrain the geometry of thrust faults and folds. The location and orientation of the modeled cross section (Figure 16) was chosen to meet the following criteria: 1) Maximum exposure of Jurassic strata along the line. 2) Consistency and representative nature of the structural orientations. 3) Regime X was avoided due to the drastic difference of structural orientation compared to other regions.

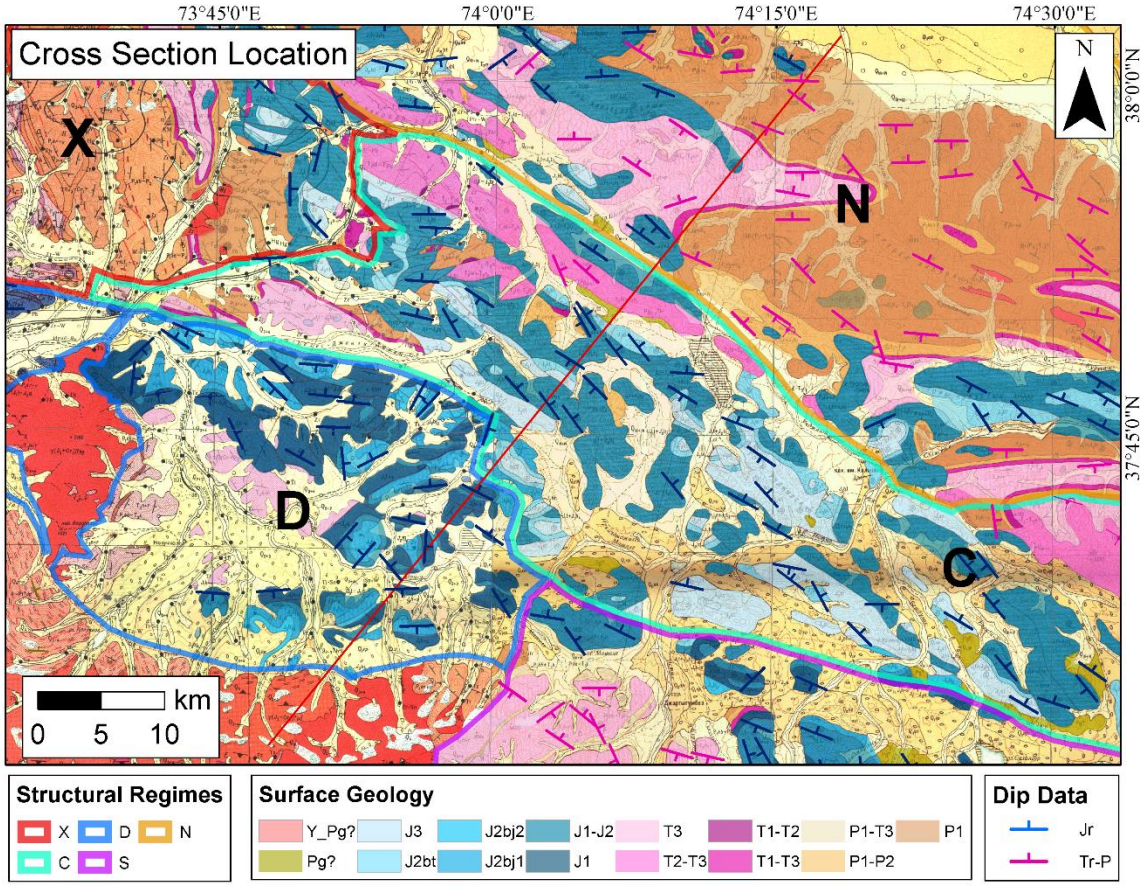

Figure 16: Location of the forward modeled cross section as indicated by the red line.

The orientation of the cross section line was determined by: 1) Dip azimuth data analyzed in MOVE to orient the line coincident with dip trends, which served as a proxy for maximum principle strain. 2) Bedding contacts from the 1:200,000 Soviet Geologic maps which were used to help orient the cross section perpendicular to bedding planes and coincident with dip direction.

4. Kinematic Cross Section

4.1. Interpretation of Geology

The primary source of surface geologic information used in this study is a series of 1:200,000 geologic maps published by the Russian Geological Research Institute (Yushin et al., 1964). For the purpose of this study, these geologic maps were evaluated using Google Earth to confirm bedding dips and make adjustments to surface geologic age interpretations where necessary. While much of the Soviet geologic maps appear consistent with relations observed in Google Earth, I made three significant reinterpretations of the geologic relationships along the cross section line based on bedding dip orientations, continuity of lithologic character/color across an area, and similarity of lithologic character/color across separated areas. In general, it appears that the interpretations on the Soviet maps (Figure 17A) exaggerate the bedding dips and as a consequence had more continuous panels of section at the surface, while my reinterpretation (Figure 17B) often called for shallower dips. Figure 18, 19, and 20 show the oblique view of the surface imagery and topography from Google Earth. View A displays the Soviet geologic interpretation, View B removes all interpretation, and View C shows my reinterpretation. The red line in these figures marks the location of the cross section.

In Figure 18 the darker blue refers of rock of age J1 the two lighter blues denotes of J1-J2 and J2 respectively. In general, the reinterpretation calls for less faulting and lower bedding angles than interpreted in the soviet maps.

In Figure 19 the darker blue refers to rock of age J1-J2 and lighter blue denotes unit J3. The peaks at NE portion of the view appear to be the same unit as the peaks seen in in the SE portion of the view. The units previously interpreted as J1-J2 I interpret to be J3. The valley floor in the center of the view has also been reinterpreted as a continuation of J2 as opposed to J3. The valley floor and J3 peak at the right side of the image appears to have a very low dip.

In Figure 20 the darker blue refers to rock of age J1-J2 and the pink refers to rock of age T2-T3. In my reinterpretation this structure is a continuous J1-J2 anticline possibly cored by Triassic material rather than a pop-up of Triassic age material.

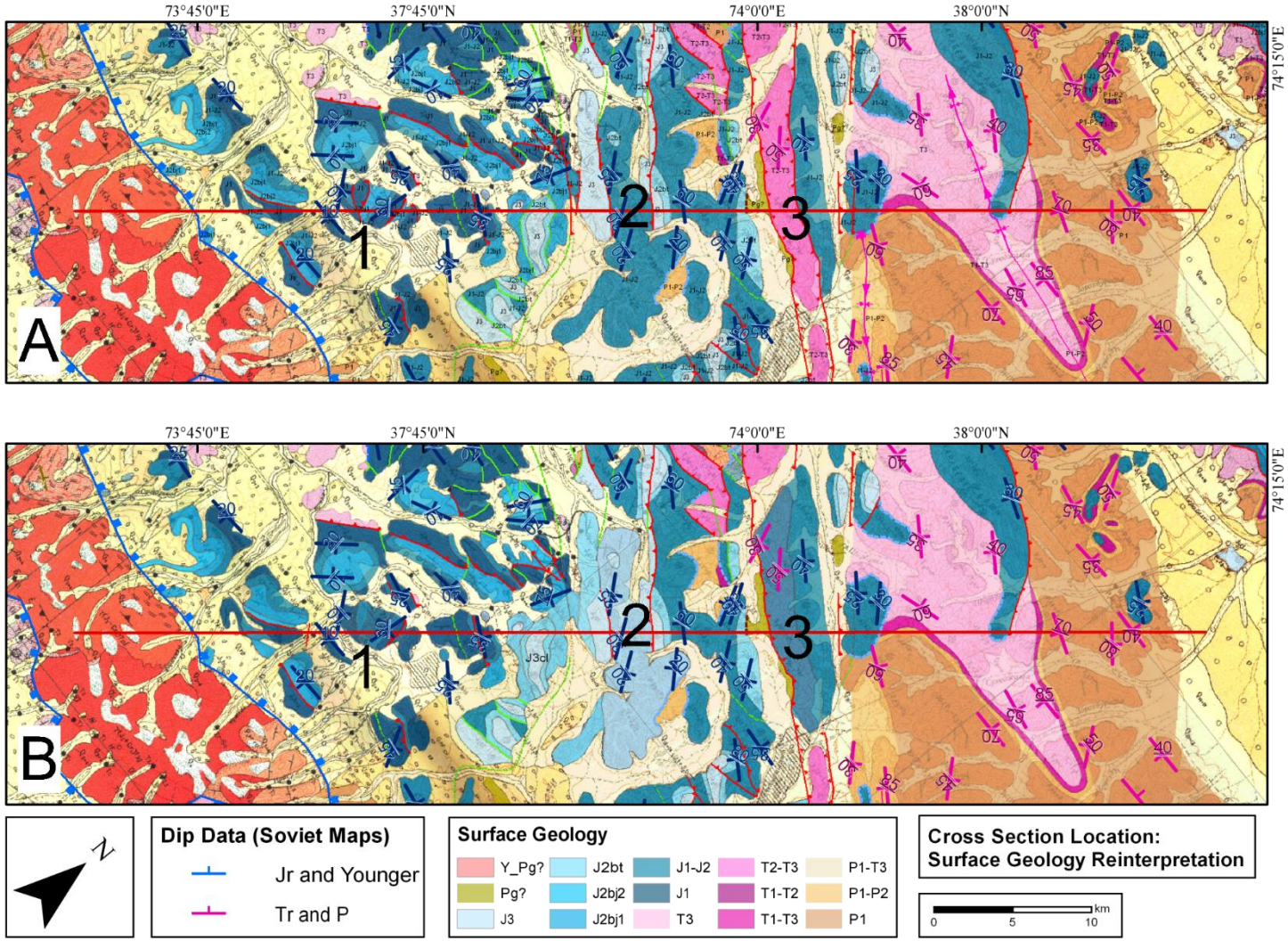

Figure 17: A) The original Soviet interpretation. The numbers 1, 2, and 3 are the main areas of reinterpretation. B) My reinterpreted surface geology from the 1:200,000 Soviet Geologic Maps used in the construction of the forward modeled cross section.

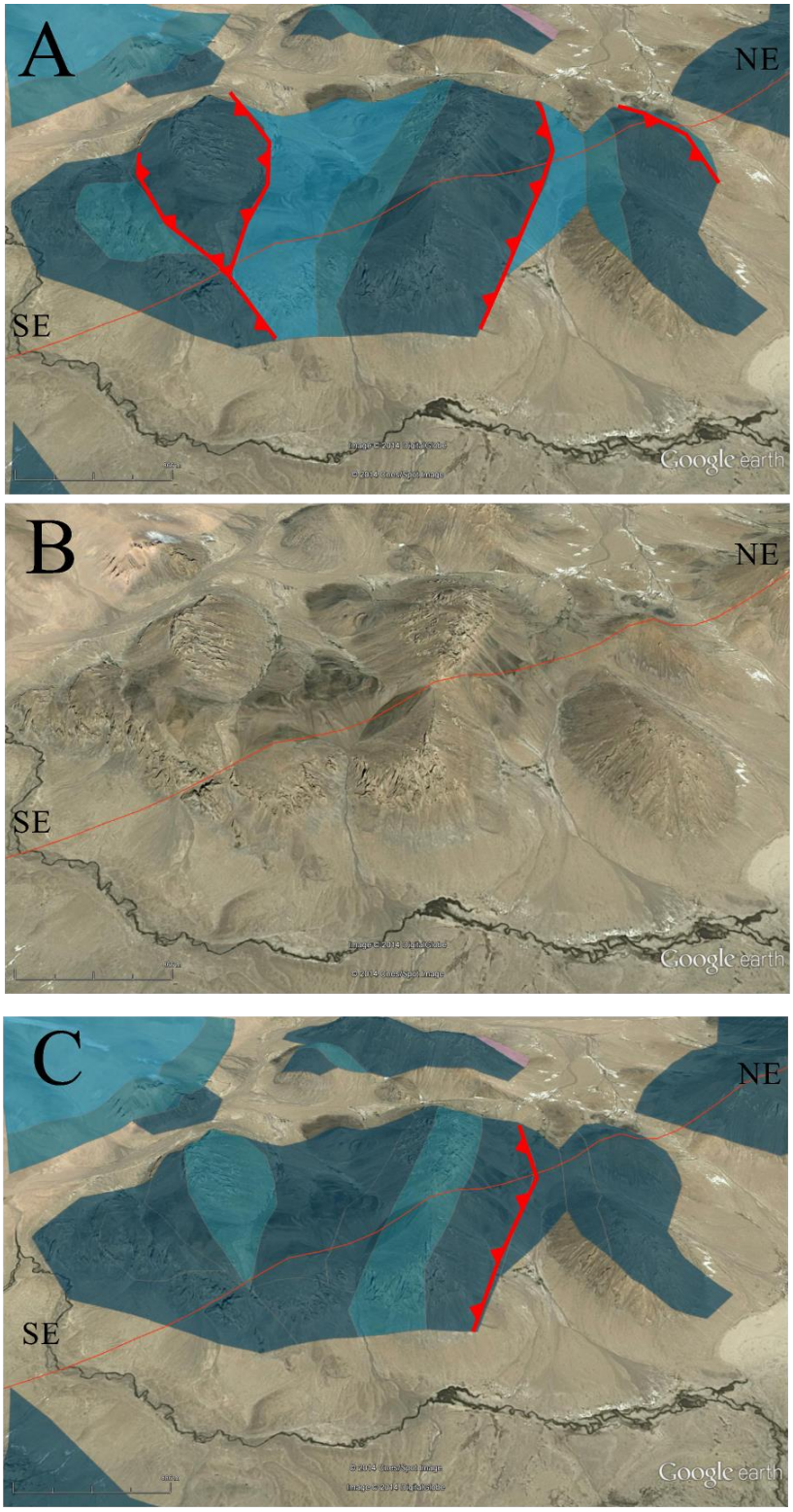

Figure 18: A) Soviet interpretation on Google Earth; B) uninterpreted Google Earth; C) my reinterpretation on Google Earth. Location shown in Figure 17. Thin red line shows the position of the cross section.

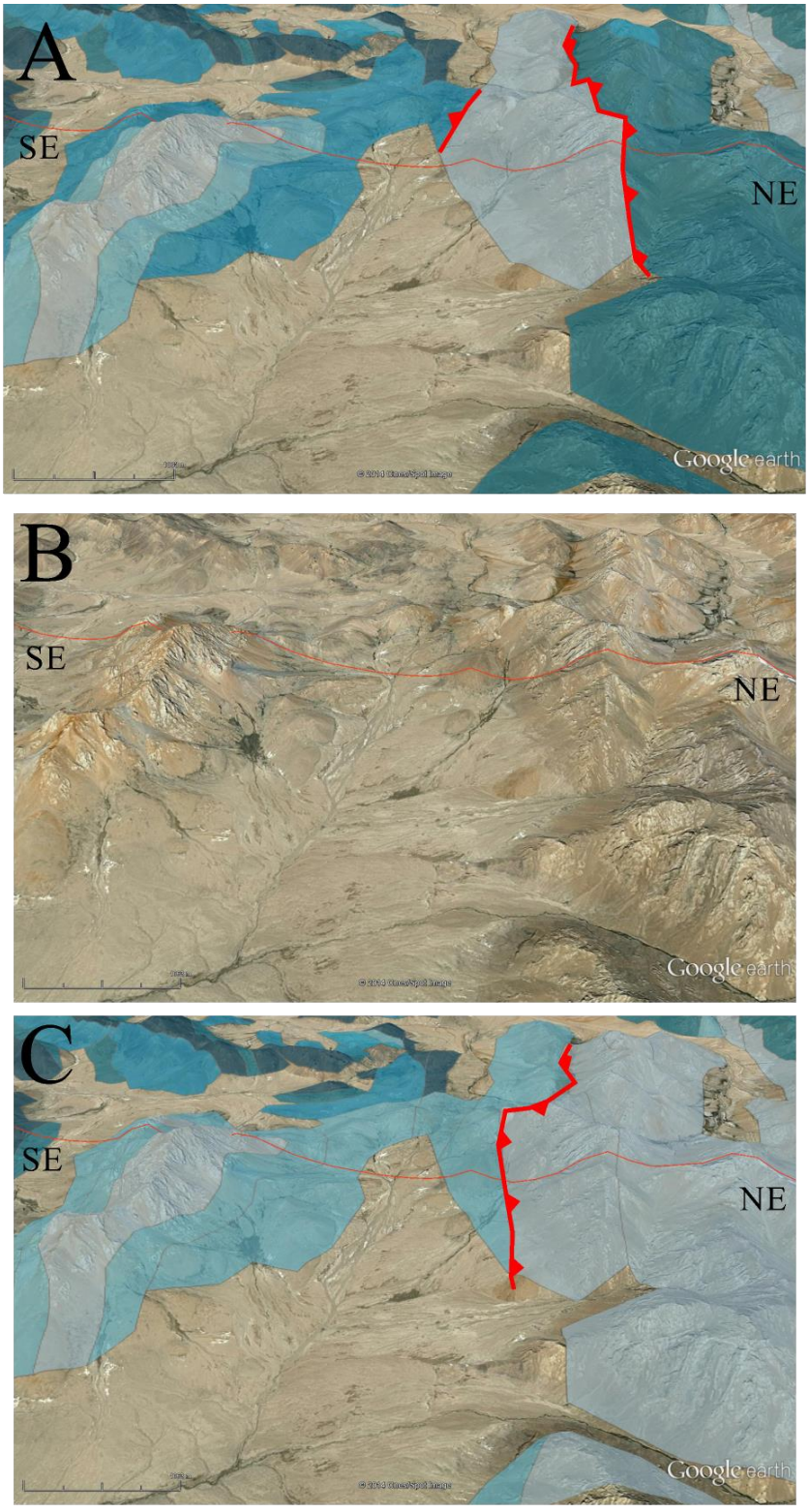

Figure 19: A) Soviet interpretation on Google Earth; B) uninterpreted Google Earth; C) my reinterpretation on Google Earth. Location shown in Figure 17. Thin red line shows the position of the cross section.

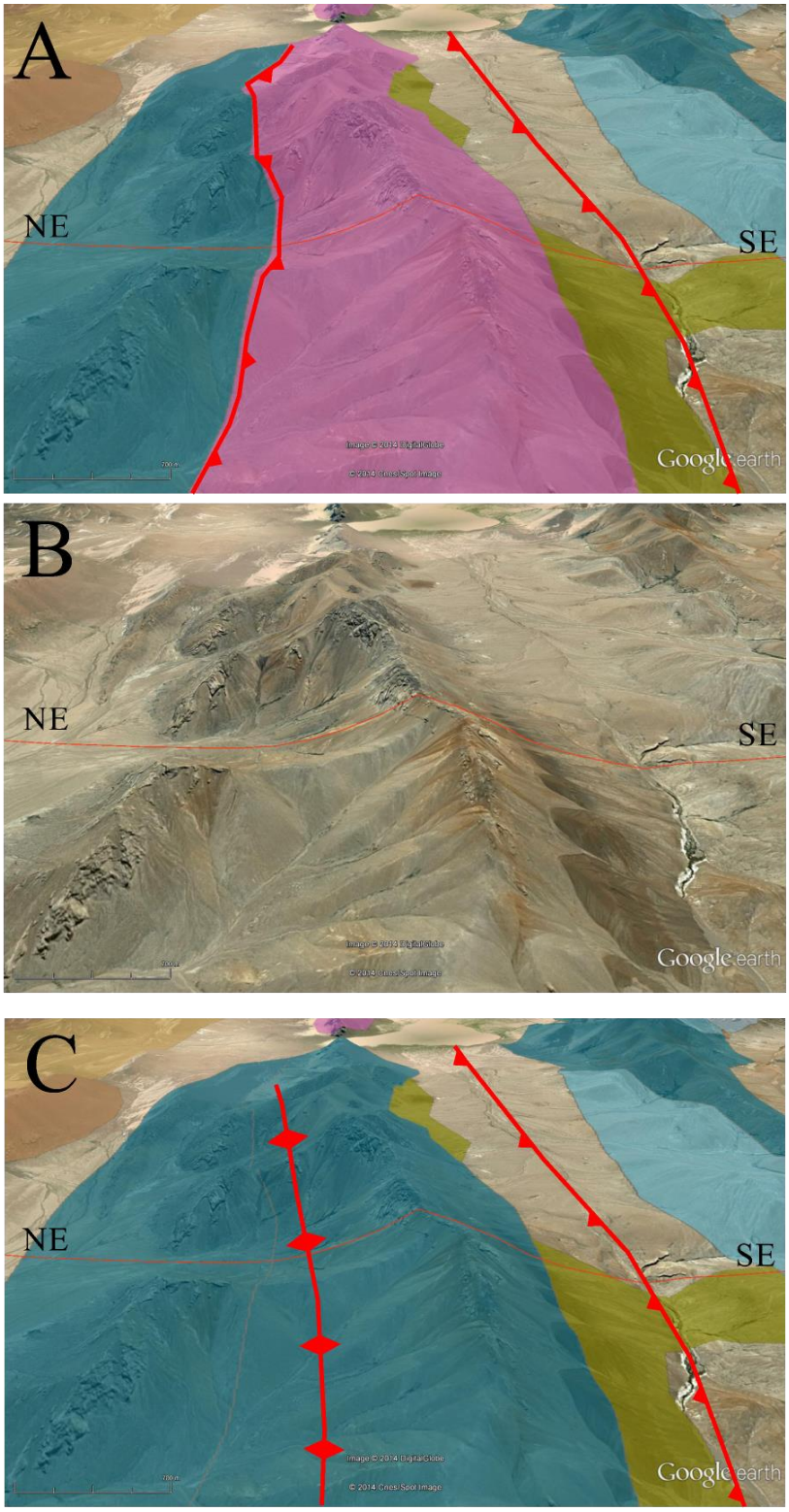

Figure 20: A) Soviet interpretation on Google Earth; B) uninterpreted Google Earth; C) my reinterpretation on Google Earth. Location shown in Figure 17. Thin red line shows the position of the cross section.

4.2. Kinematic Modeling: Assumptions and Uncertainty

Several assumptions were made in the construction of my forward modeled cross section, including the architecture of the initial condition of the model as well as the kinematics of the model's progression. The model, as constructed, serves the purpose of providing a fairly robust estimate for magnitude of horizontal shortening. It is believed that further information of the regional geology would have minimal impact on the general conclusions in regards to magnitude of shortening, gross structural style, and gross detachment levels.

A number of assumptions and uncertainties are inherent in the model parameters that were used to define the initial conditions of the model: 1) Undeformed state: The initial conditions for the model assumes a roughly layer-cake type geometry of the different geologic units. In reality the thickness of the units likely varies over the length of the cross section. 2) Unit thicknesses: The thicknesses of the units was estimated based on the stratigraphic column from the 1:200,000 Soviet Geologic Map J-43-XXI, XXII, XXVII, XXVIII and observations from the Soviet Geologic Maps. Actual unit thicknesses likely vary from these values. 3) Changes in unit thickness along section: Soviet units J1 and J1-J2 appear to change thickness over the length of the cross section. The actual geologic mechanism for the interaction between these two units is unknown. For this model, it is assumed that the changing thickness is a facies change with unit J1 pinching out to the north. 4) Initial state of the Lower Jurassic Unconformity: The model assumes that the top of the Permian-Triassic section, defined by a major unconformity, was flat at the time of Jurassic deposition and at the initial state of the model. This surface was likely more complicated, involving paleo-topography influenced by

deformation of the P-Tr section and possible normal faulting related to the lowering of the terrain to below sea level to deposit the marine Jr limestone. 5) Initial state of the basement surface: This model assumes a flat crystalline basement. It is likely the basement surface was more complex during Jr deposition. 6) Simplification of the P-Tr section: The model also depicts the P-Tr section as undeformed in the initial condition when it is known that the P-Tr had been deformed prior to the early Jr unconformity. The modeling of the P-Tr section is beyond the scope of this project and would likely have little effect on the estimates of post Jr shortening.

Assumptions and uncertainties are also inherent in the kinematics of the forward model. The following assumptions were made in regards to deformation style and detachment level. 1) Folding style and algorithm used in Move: The model primarily relies on fault bend fold type fault geometry using the simple shear algorithm in Midland Valley's MOVE software. This specific algorithm, simple shear, may not be the most appropriate of the available algorithms in Move for a compressional, fault-bend-fold, type situation. Actual fault geometry style may vary. 2) Detachment levels: The modeled detachment faults were chosen based on observed structure geometries and rock units. One of the main fault detachments utilized in this model is in the upper Permian-Triassic section (referred to as the 'Mid-Triassic' detachment in this thesis). With the P-Tr section depicted as flat in the model, these detachments appear to occur along flat lying strata. Since the P-Tr section was previously deformed, this detachment likely equates to reactivation of P-Tr structures rather than a true flat detachment on flat strata. The modeling of the Pre-Jurassic structuring of the Permian-Triassic section is beyond the scope of this study.

4.3. Kinematic Modeling: Stratigraphic Column used in Model

To constrain the initial conditions for the forward modeled cross section (Figure 21-A), I constructed a stratigraphic column and unit thicknesses (Table 1). The unit thicknesses were mostly derived from the Soviet stratigraphic column (Figure 10) with some revision based on map observations. The color shown is the color used in the forward modeled cross section (Figure 21). Observations from the Structural Regime characterization and related Google Earth observations were also used to help constrain the initial conditions.

Soviet Map Unit	Forward Model Color	Thickness Used in Model	
		Min (m)	Max (m)
J3			500
J2bt			400
J1-J2		100	500
J1		0	~550
T3			500
T2-T3			200
T1-T3			130
P1-P2			180
P1			2500
Basement			

Table 1: This table lists the geologic units and the thicknesses of these units that are used in the forward modeled cross section.

In the Structural Regime analysis, it was noted that unit J1 occurs in the southern portions of the study area on top of the Jurassic unconformity while in the central and northern regimes (Regime C and Regime N), unit J1 is no longer present. Along the line of the cross section, unit J1-J2 is present in the southern portion (Regime D) on top of unit J1 but appears to be thin (~100 m) while in the central and northern part of the cross section (Regime C and N) unit J1-J2 appears to thicken to a maximum of ~500 m and lies

directly on top of the Permian-Triassic section. This thickening and thinning of units J1 and J1-J2 was used for the initial condition of my forward model (Figure 21-A). It is possible that this inter-fingering of J1 and J1-J2 on top of the P-Tr section represents a facies change in the lowermost unit related changes from south to north after a return to marine deposition during the Jurassic.

The main detachment for the system is in the mid-Triassic. This detachment then ramps up to either a detachment on the unconformity or to a detachment in the mid Jr (Figure 21). Observations from Google Earth suggest the mid-Jurassic (J2bt) may likely be shale rich unit (slope former, darker color) making it more prone to layer parallel slip and the development of a detachment.

4.4. Kinematics: Forward Model SW-NE

The figures below show my forward modeled cross section starting from an initial condition of undeformed strata. In the initial figure (Figure 21-A), all of the faults to be used in the model are displayed. The faults are assigned identifiers based on the following criteria: The first character refers to the fault's location on the cross section (N for Northern, S for Southern). The second character refers to either the faults relative detachment level, sense of motion, or unique structural style (D for a relatively deep detachment level, S for a shallow detachment, B for back thrust sense of motion, P for fault propagation fold). The faults are then numbered by order of activation, if applicable (Figure 21-A).

The following two sections describe the progression of the mostly fault-bend fold style deformation system that verges to both the north and south onto a stable block in the middle of the cross section. This flat lying, central portion, is considered to be a structural

pin for the system and is taken as the regional elevation for the units. It is considered the regional elevation for the system because the areas to either side are deformed and uplifted (Figure 21). The deformation in the northern portion of the section is discussed separately from the southern section. The final state of the system (Figure 21-I) is then eroded down to present day topography (Figure 21-J). For ease of comparison, the final eroded state of the model is displayed side by side with the revised Soviet geologic map at the same scale for the map view and cross section (Figure 22).

4.4.1. Northern Portion of Cross Section

The structures in the northern portion of the cross section have a south-directed sense of vergence and a primary basal detachment in the mid Triassic (Base T2-T3), which is discussed first. The depth of this detachment is constrained by the structural wavelength and units involved in deformation at surface. From the observations in Figure 20, it is noted that the P-Tr section is possibly exposed in the core of the anticline formed by fault N-1. The Soviet interpretation also involves the P-Tr section in the anticline formed by fault N-2. There is also a modeled detachment on the base of the P-Tr section which acts to lift up large panels of the stratigraphic section. This deeper detachment is discussed later.

Fault N-1 has 1,300 m of shortening from a detachment in the Triassic which ramps up to the base of J2bt. This shortening is taken up by back thrusting, bringing J2bt on top of J3 on fault NB (Figure 21-B). Displacement then moves to fault N-2, a forward propagating splay of N-1. N-2 has 500 m of shortening which is taken up by backthrust NB (Figure 21-C). Fault N-2 experiences continued displacement from the north (500 m) which is then transmitted to the shallower, forward propagating fault, NS-1 (Figure 21-

D). 300 m more of slip on fault N-2 is then transmitted to the shallower fault, NS-2 (Figure 21-E). The last 250 m of movement on the upper P-Tr detachment is taken up by a fault propagation fold in front of fault FPF which results in a minor anticline (Figure 21-F).

The north portion of the cross section shows two deeply-rooted faults (ND-1 and ND-2) that sole into detachments at the base of the P-Tr section (Figure 21-G). These two faults act to bring up large panels of stratigraphic section which create long wavelength folds. These long wavelength folds have faults on their southern limb, juxtaposing P-Tr section onto Jr Section, and preserved Jr section on the northern limb, where the hanging wall has only been transported along the flat and has not gone up the ramp (Figure 21-J). Fault ND-1 has 700 m of displacement and ramps directly to the surface (Figure 21-H). The footwall of ND-1 remains at regional level and has some preserved Jr section at the surface. Fault ND-2 has 1000 m of displacement and ramps to a detachment at the base of the mid-Jurassic (Jbt2) creating a fault-bend fold anticline in J1-J2 (Figure21-I). This fault then daylights in a valley.

4.4.2. Southern Portion of Cross Section

The southern portion of the study area has a northward sense of vergence. This portion of the cross section involves the same mid-Triassic detachment as the northern portion. Shortening is accommodated primarily along two faults, S-1 and S-2. Fault S-1 has 1,500 m of shortening with detachments in the Triassic, base of the Jurassic, and a minor detachment in the mid-Jurassic (Figure 21-C). Fault S-2 has 500 m of displacement with detachments in the Triassic and base of the Jurassic (Figure 21-D). There is a total of 2,000 m of displacement along the mid-Triassic basal detachment.

The southern portion of the cross section also appears to require basement-involved faulting on SD-1 (Figure 21-G), unlike faults ND-1 and ND-2 in the northern portion which are detached at the base of the P-Tr section. A basement involved fault provides the longer ramp needed to lift the entire southern portion of the cross section above the regional level, as defined by the central portion of the cross-section. There is approximately 950 m of movement along fault SD-1. Fault SD-1 ramps from basement through the P-Tr section and steepens before it soles into a detachment on the Tr-J unconformity. This steepening of the fault acts to steepen the backlimb of the small anticline, as observed at the surface. The movement along SD-1 is then taken up along backthrust SB which repeats the units J1 and J1-J2 with appropriate dips to match surface observations (Figure 21-I).

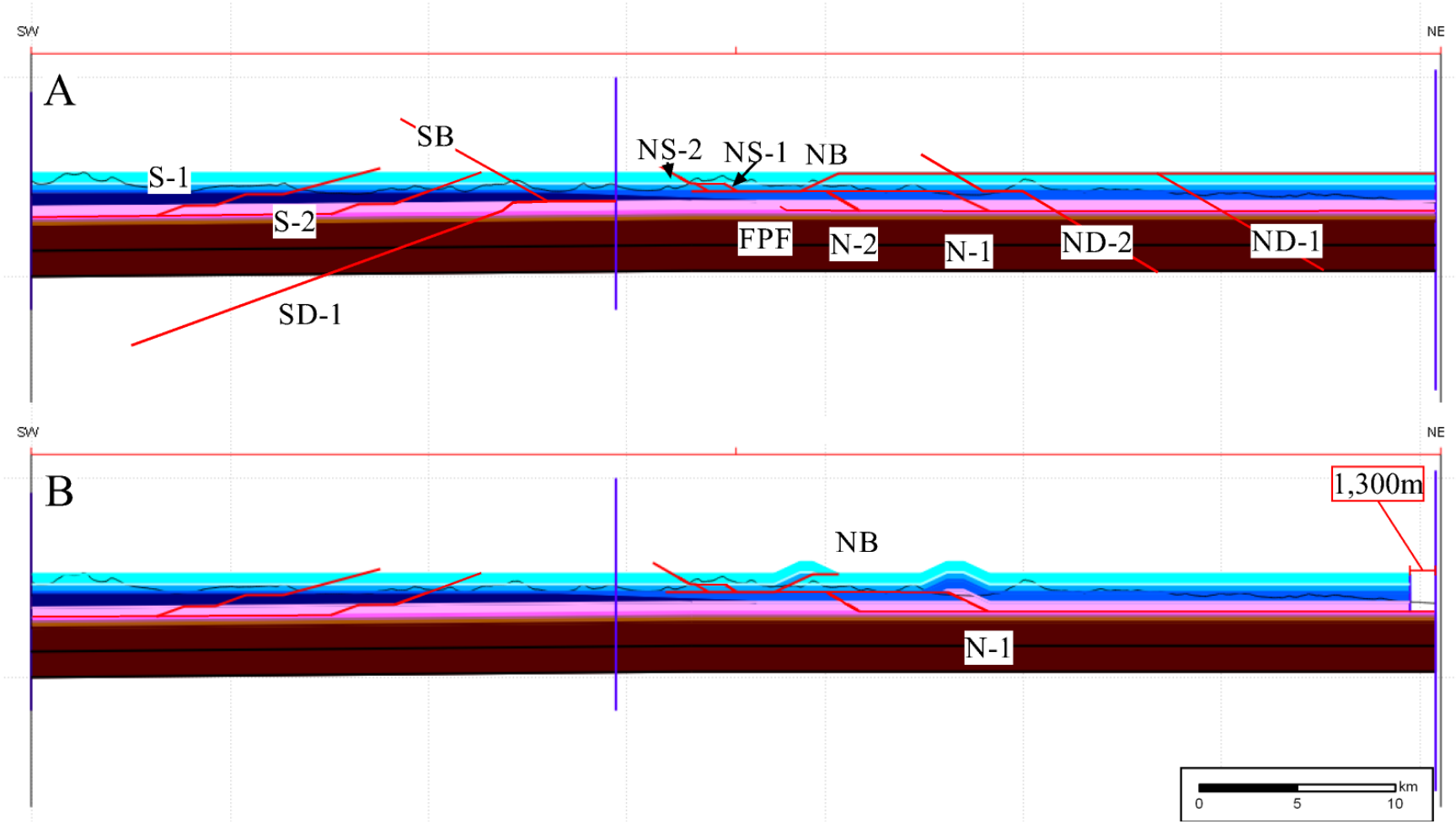

Figure 21: A) Initial condition with all faults labeled. B) Model Step 1. Displacement along faults N-1 and NB. Table 1 serves as the key for geologic unit ages.

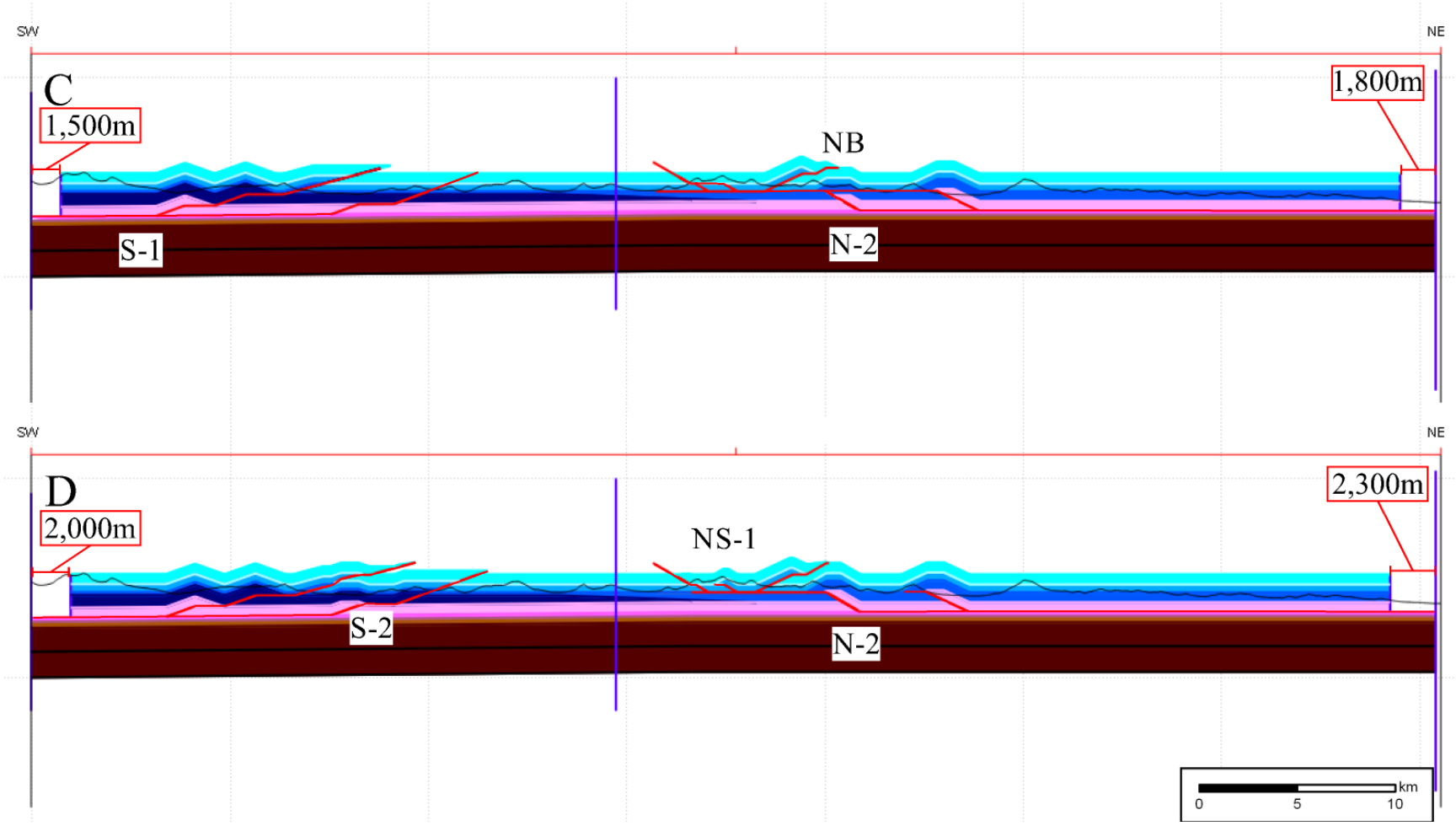

Figure 21: C) Model step 3. Activation of fault N-2 in the North, and fault S-1 in the South, D) Model step 4. Continued displacement along N-2 with activation of NS-1 in the north and activation of S-2 in the south.

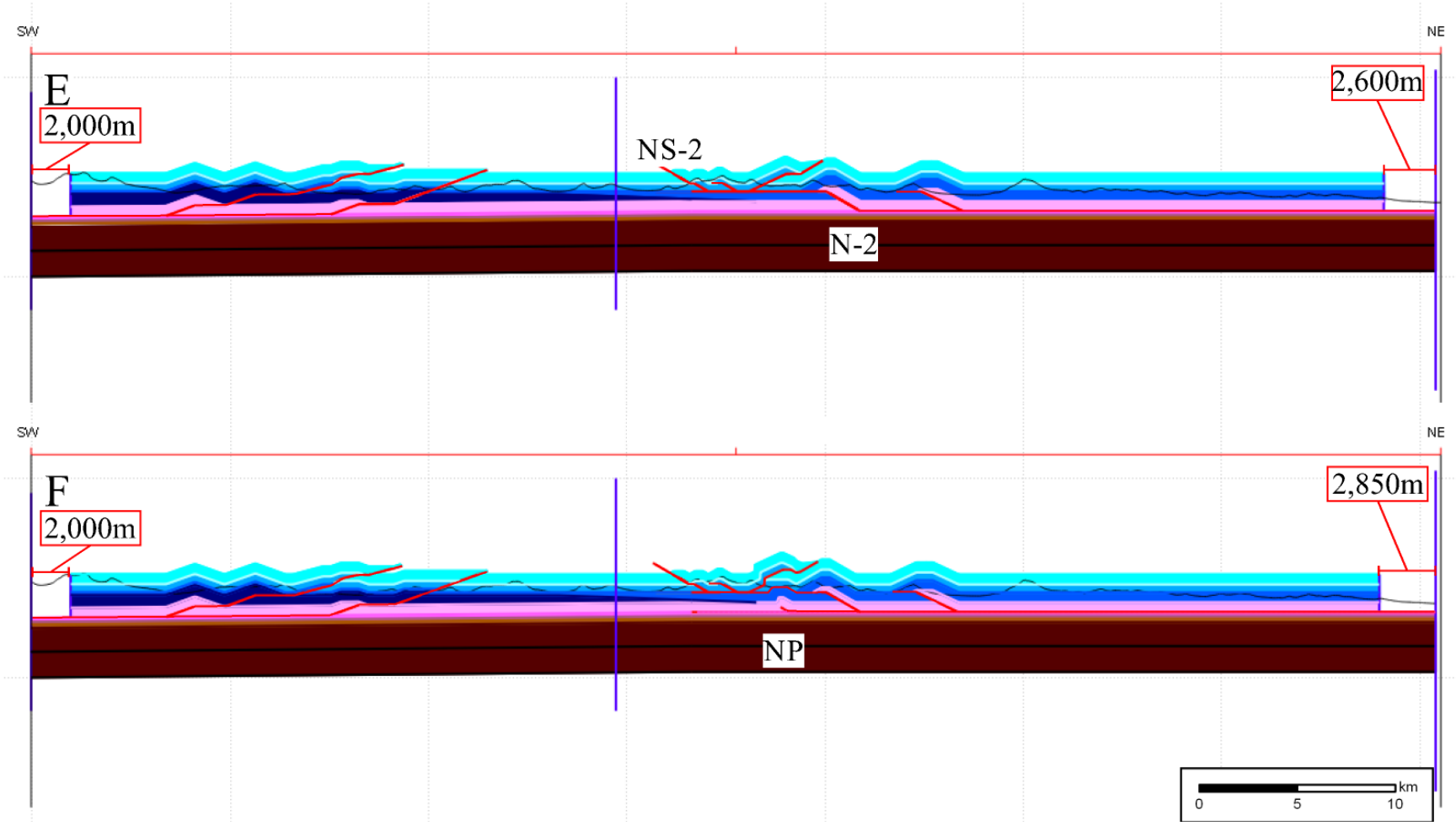

Figure 21: E) Model Step 5. Continued displacement of fault N-2 and activation of fault NS-2 in the north F) Model Step 6. Activation of fault FPF.

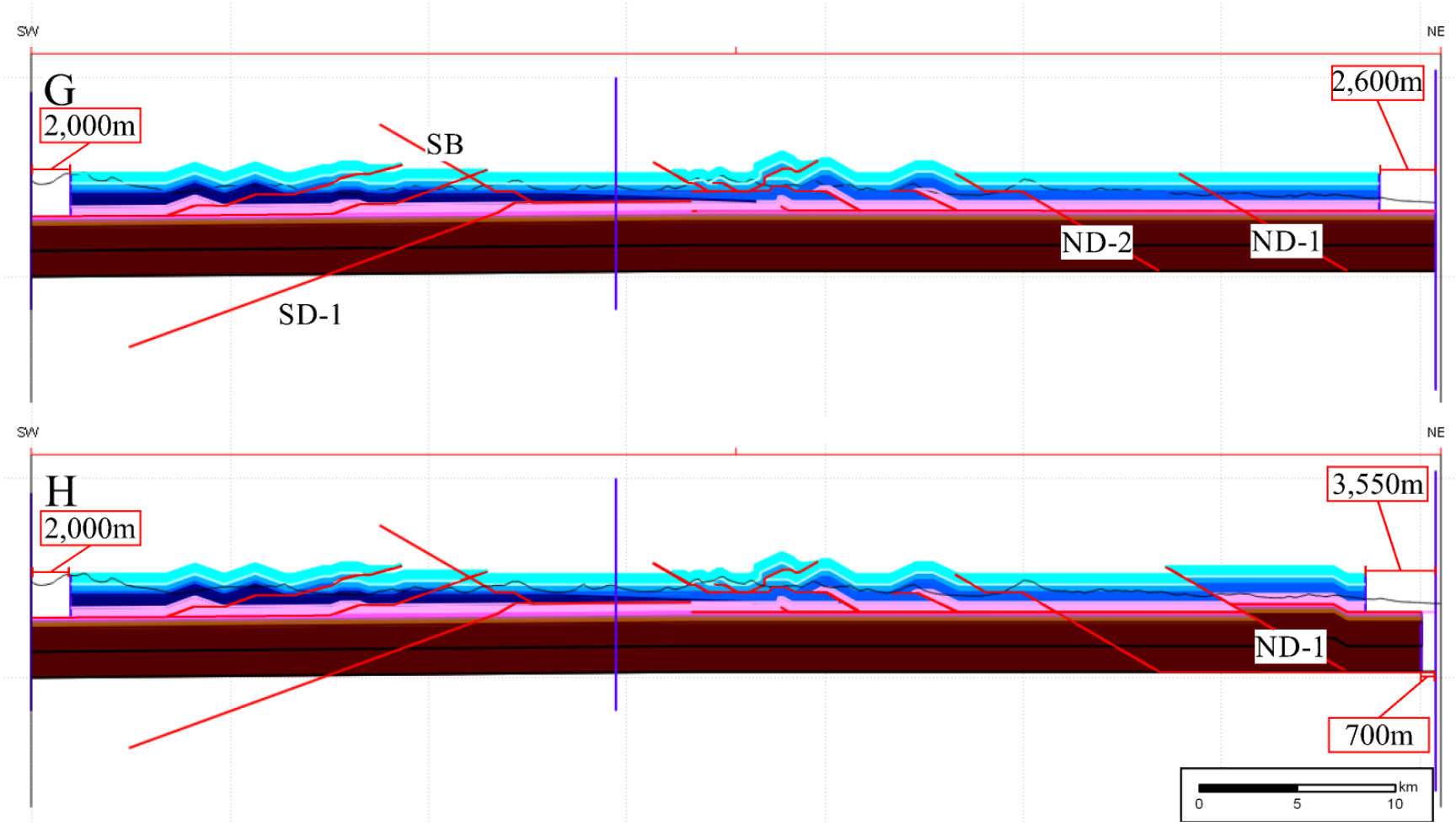

Figure 21: G) Model step 7. Displays the deeper faults with no displacement, H) Model step 8. Activation of ND-1.

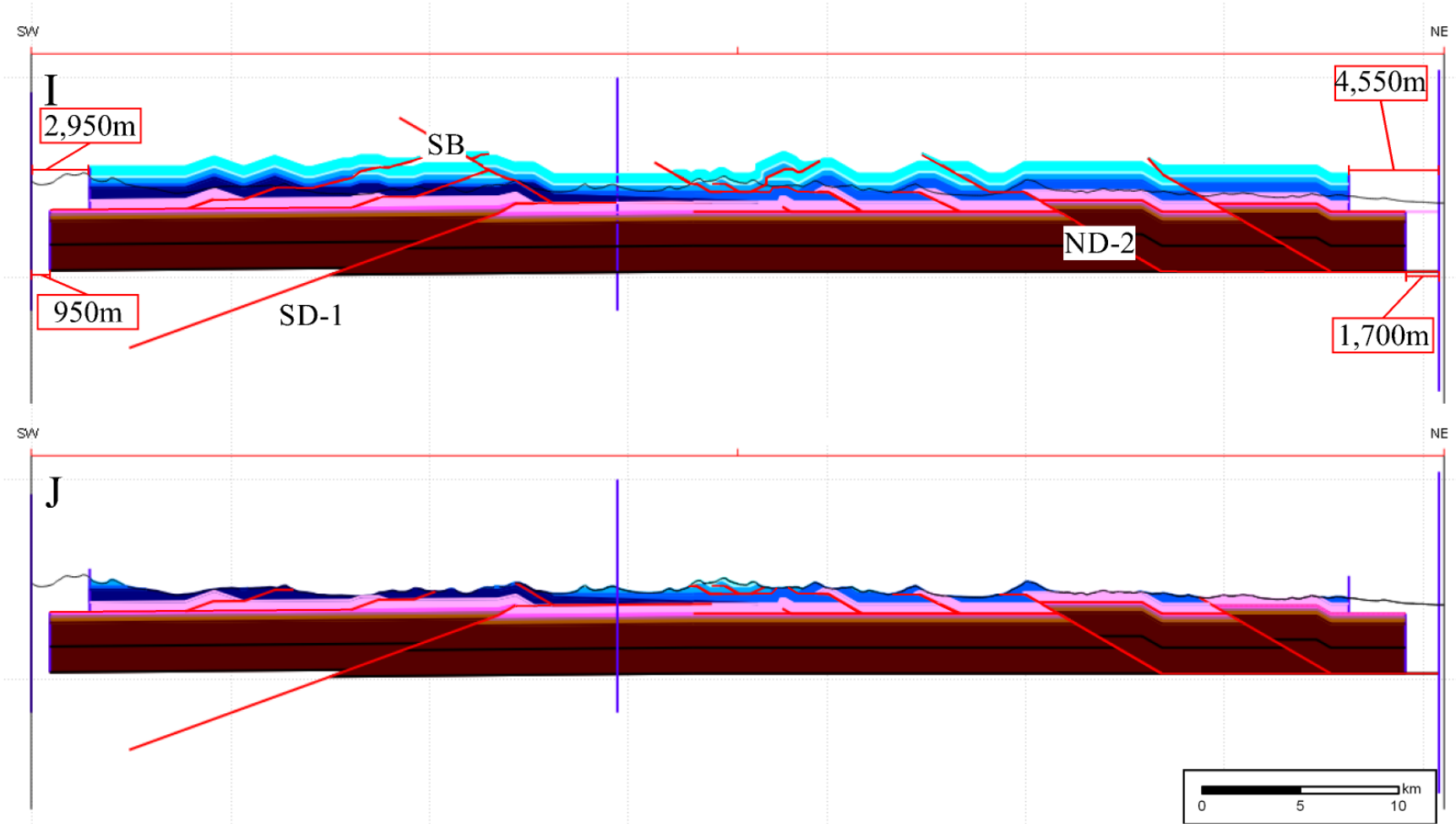

Figure 21: I) Model step 9. Displacement on fault SD-1 taken up by Fault SB, J) Model step 10. Erosion to present day topography.

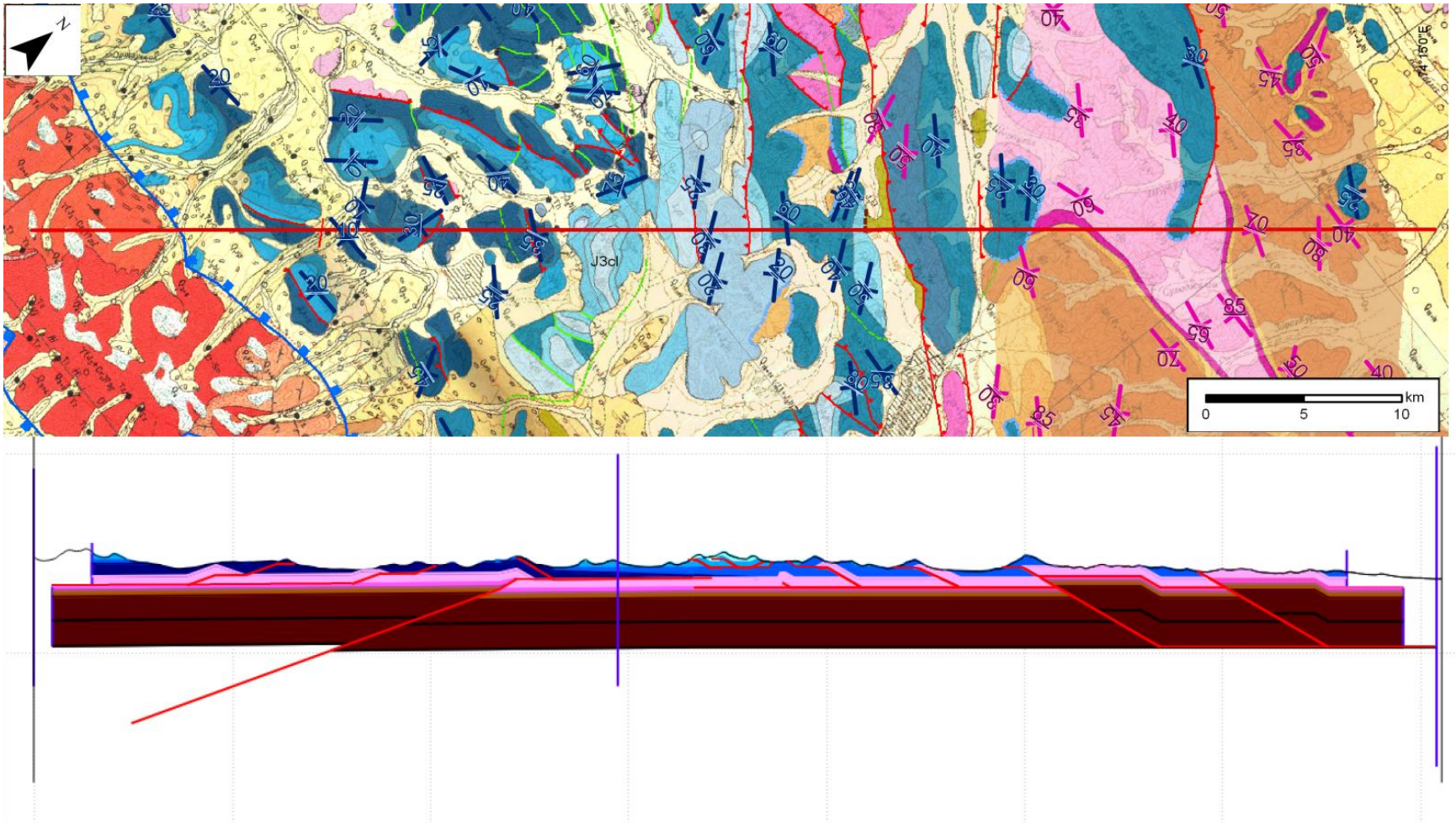

Figure 22: The final, eroded, state of the forward modeled cross section displayed at the same scale as the surface geologic map for easy comparison.

4.5. Kinematic Modeling: Shortening Results

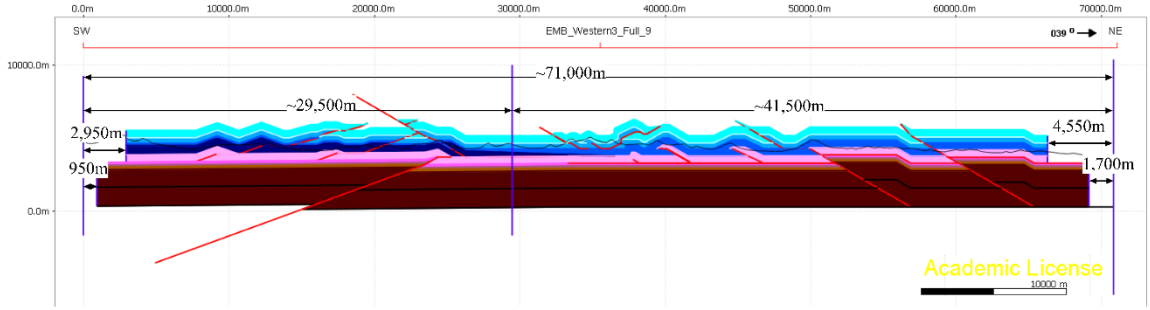

Figure 23: Final state of the forward modeled cross section with distances labeled.

Total Cross Section			
Desc.	Magnitude Shortening(m)	Undeformed Length(m)	Shortening(%)
Total	7,500	71,000	-11%
Mid -Tr	4,850	71,000	-7%
Lower	2,650	71,000	-4%
Southern Portion of Cross Section			
Total	2,950	29,500	-10%
Mid -Tri	2,000	29,500	-7%
Basement	950	29,500	-3%
Northern Portion of Cross Section			
Total	4,550	41,500	-11%
Mid -Tr	2,850	41,500	-7%
Base P-Tr	1,700	41,500	-4%

Table 2: Table of magnitude of shortening and shortening % for the total cross section, the southern portion (SW of stable central portion) and northern portion (NE of stable central portion). The total shortening for these three areas are then divided into shortening for general detachment levels (mid-Triassic detachment, base Permian-Triassic detachment or basement involved detachment). The description of "Lower" detachment referrers to a combination of the basement and base Permian-Triassic detachments for the total cross section.

The total magnitude of shortening estimated by the model is 7.5km (~11%). The total shortening can then be divided into several subsets to analyze contributions from the northern and southern portions of the section and also from various detachment levels (Figure 23 and Table 2). The equation used for percent shortening is listed below where 'e' is shortening, 'Lf' is final length, 'Lo' is original length and ΔL is the magnitude of shortening (Davis et al., 2011):

$$e = (Lf - Lo)/Lo$$

$$e = \Delta L/Lo$$

Total percent shortening in the southern section is ~10% (~3 km) with ~7% from the mid-Triassic detachment and ~3% from the basement detachment (Table 2). The southern section extends to the purple line which marks the middle of the undeformed portion of the cross section (Figure 23).

The total percent shortening in the northern section is ~11% (~4.5 km) with ~7% coming from the mid-Triassic detachment and ~4% from the base Permian detachment (Table 2). The northern section extends to the purple line which marks the middle of the undeformed portion of the cross section (Figure 23).

In regards to shortening contributions from different detachment levels, total contribution from the mid-Triassic detachment is ~7% while the deeper detachments (basement and base-Permian) contributed ~4% to the total percent shortening (Table 2).

5. Discussion

5.1. Shortening Findings and Implications to Region

Estimates of Cenozoic shortening along the Himalayan-Tibetan orogen place 50-80% more intra-Asia shortening in the western portion of the orogen than the eastern, even though ~25% more overall convergence is attributed to the eastern portion of the orogen (van Hinsbergen et al., 2012). The estimates of intra-Asia convergence in the western portion of the orogen include a large portion of shortening (~665km) in the Pamir Mountains, ~315 km due to emplacement of the Pamir salient over the Tarim-Tajik basin and another ~340 km taken up by Cenozoic internal shortening within the Southern Pamir (240 km) and Central Pamir (100 km) (Burtman and Molnar, 1993).

As previously stated, ~110 km of the southeast Pamir shortening budget related to a nappe has since been recognized as an extensional feature related to gneiss dome extrusion (Stübner et al., 2013). In addition, my study yields only ~7.5 km of Cenozoic shortening in the fold and thrust belt of the southeast Pamir, much less than the ~50 km proposed by Burtman and Molnar (1993, and references therein). With the corrections cited and proposed in this study, Burtman and Molnar (1993)'s estimate of ~340 km of Cenozoic shortening within the Pamir is lowered to ~190 km. This result indicates that intra-Asian shortening across the length of the Himalayan-Tibetan orogen during the Cenozoic may be more equal than previously estimated. Instead of 50%-80%, there may be just 30%-60% more Cenozoic shortening in the western Himalayan-Tibetan orogen as compared to the central and eastern portions respectively (Figure 24). Since the total amount of convergence between the Indian and Eurasian plates has not changed, the

amount of shortening removed from the ‘intra-Asia collision’ (green bar in Figure 24) must then be added to the ‘missing’ convergence category (red bar in Figure 24).

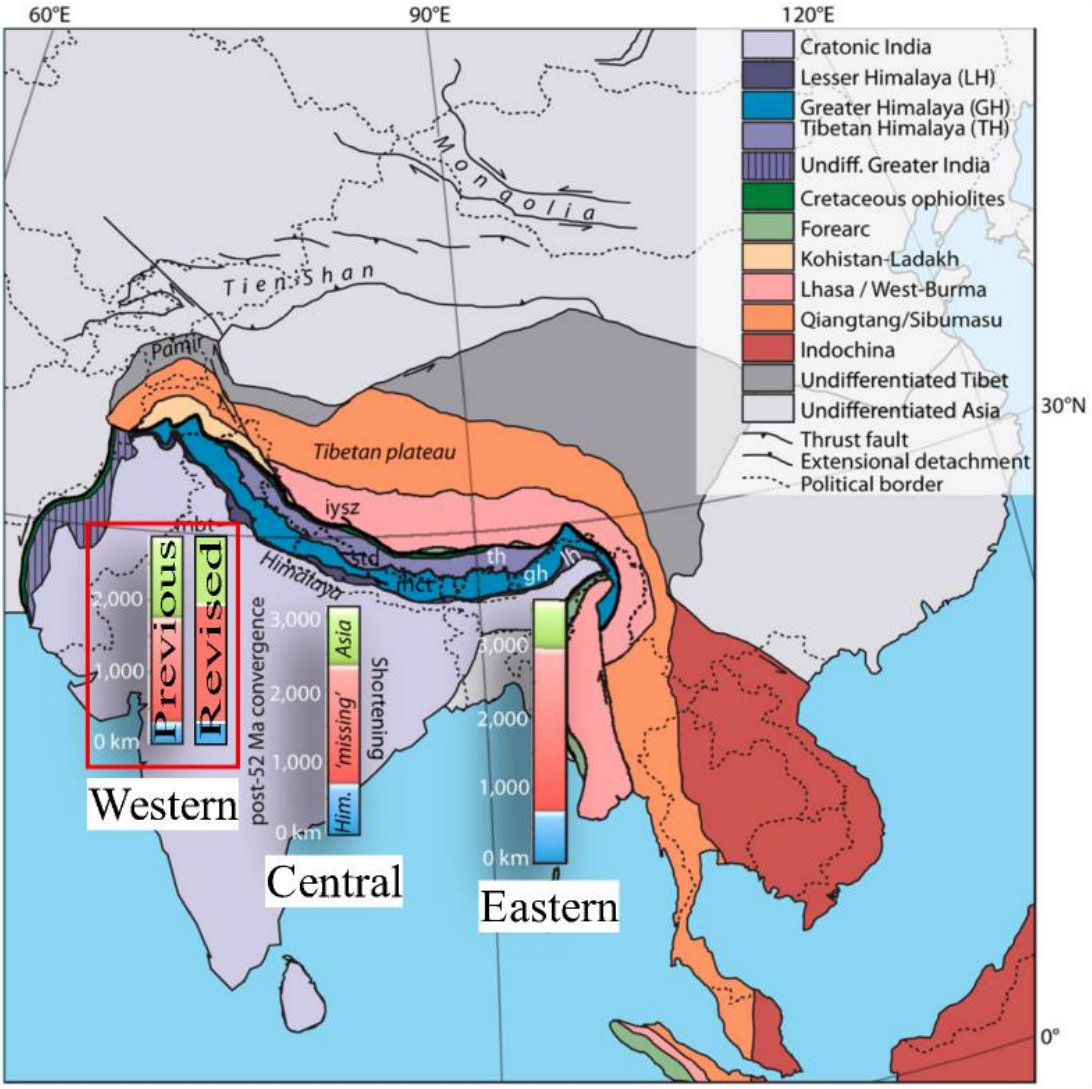

Figure 24: Total amount of convergence attributed to different portion on the India – Asia Collision zone. The green portion of the bar accounts for intra-Asia collision, the red portion represents ‘missing’ shortening, and the blue portion is Himalayan shortening(van Hinsbergen et al., 2012). The two bars on the left side of the portion represent the previous estimates of convergence as presented by van Hinsbergen et al., 2012 and the revised estimate of convergence.

5.2 Shortening and Implications on Crustal Thickness

Removing a significant amount of shortening also has implications for the crustal thickness of the Pamir prior to Cenozoic deformation. The initial crustal thickness can be estimated using present day width, thickness, and estimated magnitude of Cenozoic internal shortening for the Pamir Mountains. The current north-south width of the Pamir Plateau was measured from the Alai thrust in the north to the Afghanistan-Pakistan border to the south giving a current width of 271 km (Figure 25). Mechie 2011 modeled the current crustal thickness along a profile in the Pamir and found a range from 65.5 km beneath the southern Pamir to 73.6 km thick in the northern Pamir (Mechie et al., 2011). For the purposes of this exercise, an average crustal thickness of 70 km was used. The previous and revised estimates of Cenozoic internal shortening were used to constrain the width of the Pamir prior to Cenozoic shortening. A simple area balance was then used to estimate pre-Cenozoic crustal thickness.

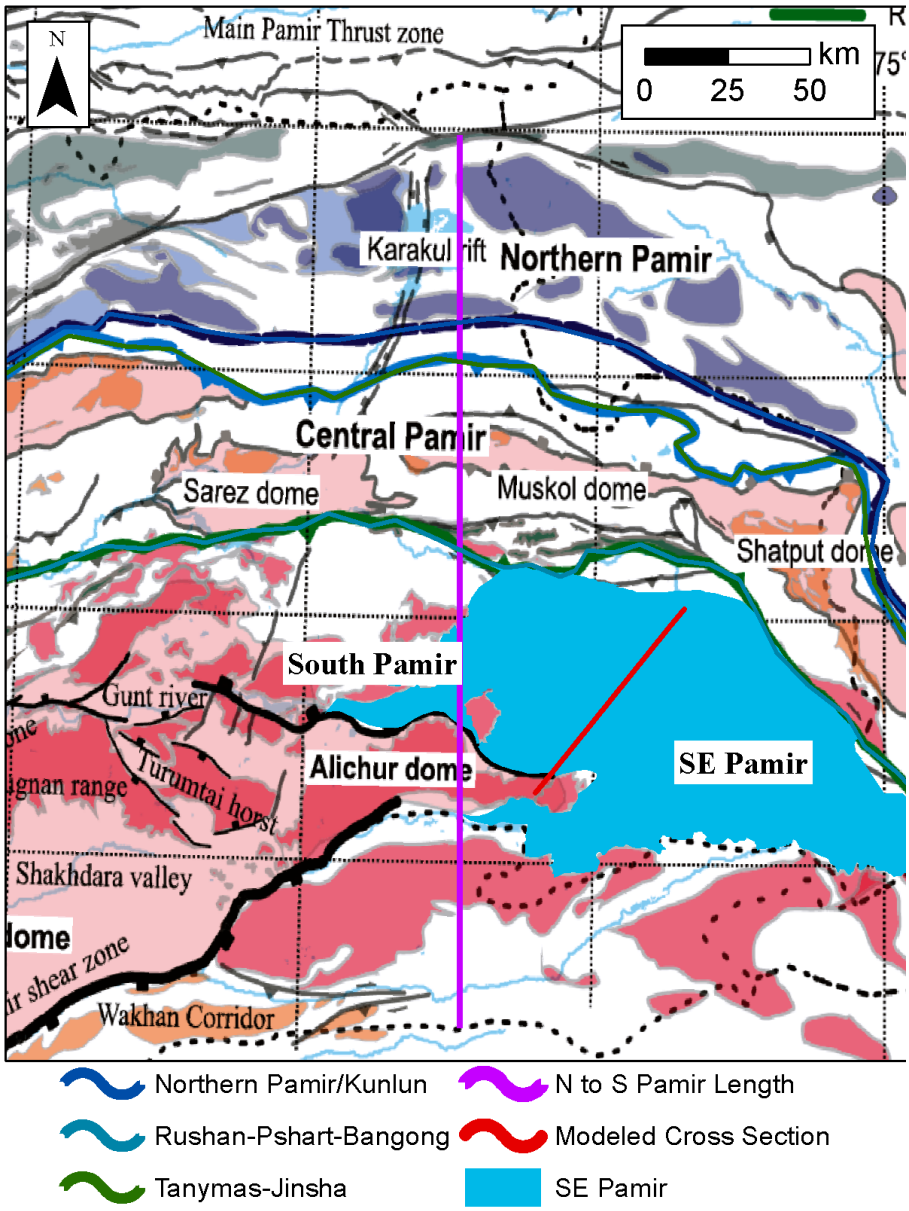

Figure 25: Map view of the Pamir Range modified from Stubner et al., 2013(Stübner et al., 2013).The blue polygon represents the SE Pamir (area of interest) with the location of the modeled cross section and an arbitrary profile extending representing the length from the N Pamir to S Pamir

Figure 26 graphically shows the area balance used to calculate the initial thickness based on the Burtman and Molnar 1993's estimate of ~340 km of internal shortening (previous initial condition) and the revised estimate of ~190 km (revised initial condition). A current thickness of 70 km (Mechie et al., 2011) and width of ~271 km

(Figure 25) were used. The approximate cross sectional area of the current Pamir is 18,970 km^2. This area yields a crustal thicknesses of 31 km for the previous estimate of shortening (~340km; (Burtman and Molnar, 1993) and 41 km for the revised estimate of shortening (~190 km).

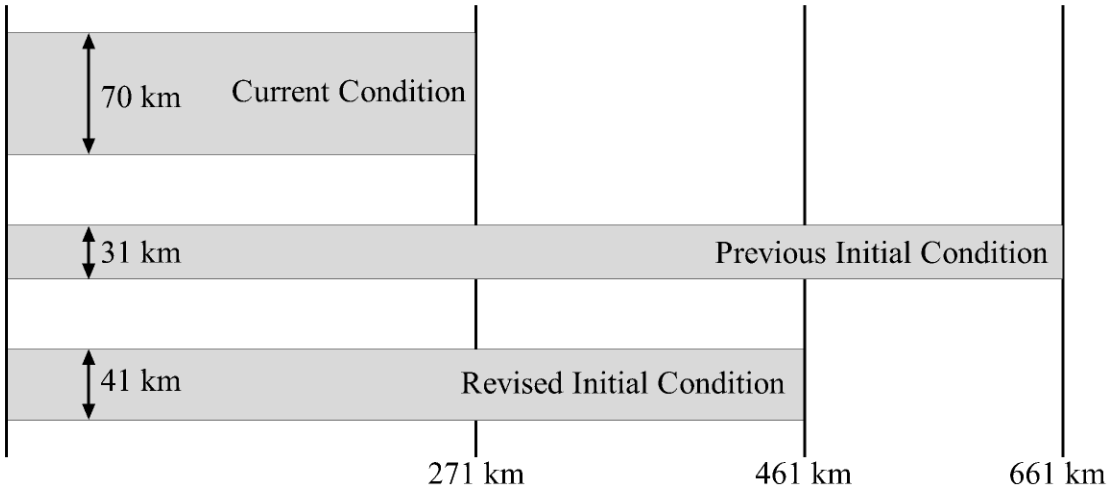

Figure 26: Graphical representation of the area balance used to estimate pre-Cenozoic crustal thickness of the Pamir. 'Current Condition' represents the present state of the Pamir. "Previous Initial Condition' represents the pre-Cenozoic length and thickness of the Pamir based on Burtman and Molnar 1993's estimates. 'Revised Initial Condition' represents the pre-Cenozoic length and thickness based on the revised estimates of shortening cited and estimated in this study.

Crustal Thickening	Magnitude or %
Final Length	271 km
Final Thickness	70 km
Initial Length, Previous	611 km
Initial Thickness, Previous	31 km
% Shorteneing, Previous	-56%
Initial Length, Revised	461 km
Initial Thickness, Revised	41 km
% Shortening, Revised	-41%

Table 3: This table lists the length, thickness, and shortening percentages associated with the present state of the Pamir (Final Length), Burtman and Molnar 1993's pre Cenozoic state (Initial Length, Previous), and the revisions suggested in this study (Initial Length, Revised).

This model assumes a constant area of material with no material being lost from the surface by process such as erosion and denudation, and no material being added or removed from the bottom by processes such as underthrusting, delamination, subduction, or under plating. The ends of the block of material do not change shape through thrusting or underthrusting which would change the length of the section. This estimate suggests that either 1) the pre-Jurassic Pamir crust was thicker than previously thought, or 2) a crustal thickening method other than post-Jurassic bulk shortening contributed to the present crustal thickness.

5.2.1. Thicker Crust before Post-Jurassic Shortening

Airy isostasy calculations show that a thicker section of continental crust will sit at a higher elevation due to buoyancy forces and the density differences between continental crust and mantle material. However, the deposition of the Jurassic marine carbonates on top of the unconformity suggests a crustal thickness of less than 30-35 km in order for the region to be at/below sea level. This implies that the thickening due to post-Jurassic bulk shortening is not enough to produce the presently observed crustal thickness.

5.2.2. Thicker Crust after Post-Jurassic Shortening

Underthrusting and underplating, related to the complex subduction beneath the Pamir, is the most likely mechanism to increase the thickness of the SE Pamir. As the terranes of the Pamir have advanced 315km onto the Eurasian Plate, the continental lithosphere of Eurasia has underthrust the Pamir (Burtman and Molnar, 1993; Koulakov and Sobolev, 2006; Sobel et al., 2013). Tomographic imaging shows that the Eurasian lithosphere has been subducted and is dipping to the east beneath the western Pamir and to the south beneath the northern Pamir (Sippl et al., 2013). As this crust is underthrusting

the Pamir, different layers of the subducting lithosphere may be delaminating, with the upper crust underplated beneath the Pamir and the lower crust and mantle lithosphere continuing to be subducted into the mantle (Sippl et al., 2013).

To investigate underthrusting, the amount of crustal thickness missing from my model was calculated. Assuming the same length of crust as used above with a normal thickness of ~30 km was shortened 190km to the present day length, it would have a thickness of ~52 km. This is ~18km thinner than the present day thickness. This suggests that ~18km of upper crust of the subducting Eurasian Plate has delaminated and underthrust the Pamir to increase crustal thickness.

5.3. Detachment Levels

Previous work has suggested that the deformation of the pre- and post-Jurassic shortening events, separated by a major angular unconformity, were are at oblique angles to each other (Angiolini et al., 2013) implying that the shortening of the P-Tr and post Early Jurassic sections were separate events in time. It was expected that the lower Jurassic unconformity and the red beds of the Darbash Group that lie on top of this unconformity, was a major detachment for the shortening of the Jr section since the two deformation events were thought to be at oblique angles making reactivation of the structures in the P-Tr section unlikely. My modeling suggests the unconformity acts as a detachment, but it is not the main regional detachment. Instead, my modeling suggests there are several other detachment levels required to produce the structures presently seen at the surface.

A major detachment level is required within the P-Tr section. This suggests reactivation of older structures within the P-Tr section. Dip analysis also shows the

relative angle of the structures within the P-Tr and Jr sections are actually coincident with one another, within 1° to 5°, throughout most of the SE Pamir (Figures,12-15). This would be consistent with reactivation of the P-Tr structures during Cenozoic shortening event.

Deep detachments at the base P-Tr section and in the basement are required to bring large panels of section to an above-regional elevation. Such a deep seated thrust could possibly be from the inversion of normal faults formed during the rifting from Gondwana in the late Carboniferous to early Triassic (Zanchi and Gaetani, 2011; van Hinsbergen et al., 2012; Angiolini et al., 2013).

5.4. Structural Style / Dual-Vergent Thrust System

In order to model the geologic structures presently seen at the surface, dual vergence is required from both the NE and SW onto a relatively undeformed (flat lying) section. This does not appear to be a classic fold and thrust belt with a dominent sense of vergence and a defined propagating deformation front. Instead, this deformed section appears to have a stable structural area in the center of the section which experienced shortening from both sides. Beyond the extent of the cross section, the shortening feeds into the Rushan-Pshart zone to the north and Karakoram to the south.

6. Conclusion

In this study, the Jurassic carbonates of the SE Pamir were used as a strain marker to evaluate post-Jurassic deformation. A forward modeled cross-section was constructed across the region to estimate the magnitude of shortening, the depth of detachment, and the structural style in this area.

In order to recreate present-day structural deformation, my model requires several detachment levels and a dual sense of vergence. My results suggest vergence to both the southwest and northeast onto a stable structural area in the middle of the cross section. This stable panel of section represents the regional elevation for the deformed horizons. Modeling also suggests that several levels of detachment are needed to produce the deformation observed at the surface. One of the major levels of detachment is interpreted to be in the upper P-Tr section suggesting reactivation of older structures within this section. Deeper detached faults are also required to uplift large panels of section above the regional level. Strike and dip analysis of the Permian-Triassic section, when compared to the Jurassic units, suggests that the structural orientation of the two units may be more coincident than previously recognized in the Southeast Pamir.

My modeling suggests that the Jurassic units of the SE Pamir have experienced ~7.5 km shortening, much less than the existing estimate of 50 km of Cenozoic shortening for the SE Pamir. This implies that the Cenozoic intra-Asia convergence across the Himalayan-Tibetan Orogen may be more equal than currently recognized. This result also implies that a process other than horizontal bulk shortening, most likely underplating, from the north or south is required to account for the current crustal thickness of the Pamir.

7. References

Angiolini, L., Zanchi, A., Zanchetta, S., Nicora, A., and Vezzoli, G., 2013, The Cimmerian Geopuzzle: New Data from South Pamir: Terra Nova, v. 0, no. 0, p. 1-9.

Burtman, V. S., and Molnar, P., 1993, Geological and Geophysical Evidence for Deep Subduction of Continental Crust beneath the Pamir, Volume 281: United States, Geological Society of America (GSA) : Boulder, CO, United States.

Davis, G. H., Reynolds, S. J., and Kluth, C. F., 2011, Structural Geology of Rocks and Regions, 3rd Edition, Wiley.

Dronov, V., 2006, Stratigrafiďeskij Slovar'pamira, Technische Universität Bergakademie Freiberg.

Garzanti, E., Andò, S., and Vezzoli, G., 2006, The Continental Crust as a Source of Sand (Southern Alps Cross Section, Northern Italy): The Journal of Geology, v. 114, no. 5, p. 533-554.

Kapp, P., Yin, A., Harrison, T. M., and Ding, L., 2005, Cretaceous-Tertiary Shortening, Basin Development, and Volcanism in Central Tibet: Geological Society of America Bulletin, v. 117, no. 7-8, p. 865-878.

Kapp, P., DeCelles, P. G., Gehrels, G. E., Heizler, M., and Ding, L., 2007, Geological Records of the Lhasa-Qiangtang and Indo-Asian Collisions in the Nima Area of Central Tibet: Geological Society of America Bulletin, v. 119, no. 7-8, p. 917-933.

Korchagin, O. A., 2008, Foraminifers and Stratigraphy of the Karatash Group (Lower Triassic-Middle Anisian), the Southeastern Pamir: Stratigraphy and Geological Correlation, v. 16, no. 3, p. 248-256.

-, 2009, Kaeveria Fluegeli (Zaninetti, Altiner, Dager Et Ducret, 1982) (Foraminifera) from Upper Triassic of the South-East Pamirs: Stratigraphy and Geological Correlation, v. 17, no. 1, p. 62-67.

Koulakov, I., and Sobolev, S. V., 2006, A Tomographic Image of Indian Lithosphere Break-Off beneath the Pamir-Hindukush Region: Geophysical Journal International, v. 164, no. 2, p. 425-440.

Le Pichon, X., Fournier, M., and Jolivet, L., 1992, Kinematics, Topography, Shortening, and Extrusion in the India-Eurasia Collision: Tectonics, v. 11, no. 6, p. 1085-1098.

Leier, A. L., DeCelles, P. G., Kapp, P., and Gehrels, G. E., 2007, Lower Cretaceous Strata in the Lhasa Terrane, Tibet, with Implications for Understanding the Early Tectonic History of the Tibetan Plateau: Journal of Sedimentary Research, v. 77, no. 10, p. 809-825.

Mechie, J., Yuan, X., Schurr, B., Schneider, F., Sippl, C., Ratschbacher, L., Minaev, V., Gadoev, M., Oimahmadov, I., Abdybachaev, U., Moldobekov, B., Orunbaev, S., and Negmatullaev, S., 2011, Crustal and Uppermost Mantle Velocity Structure Along a Profile across the Pamir and Southern Tien Shan as Derived from Project Tipage Wide-Angle Seismic Data: Geophysical Journal International, v. 188, no. 2, p. 385-407.

Murphy, M. A., Yin, A., Harrison, T. M., Dürr, S. B., Z, C., Ryerson, F. J., Kidd, W. S. F., X, W., and X, Z., 1997, Did the Indo-Asian Collision Alone Create the Tibetan Plateau?: Geology, v. 25, no. 8, p. 719-722.

Robinson, A. C., 2009, Geologic Offsets across the Northern Karakorum Fault; Implications for Its Role and Terrane Correlations in the Western Himalayan-Tibetan Orogen: Earth and Planetary Science Letters, v. 279, no. 1-2, p. 123-130.

Robinson, A. C., Ducea, M., and Lapen, T. J., 2012, Detrital Zircon and Isotopic Constraints on the Crustal Architecture and Tectonic Evolution of the Northeastern Pamir: Tectonics, v. 31, no. 2, p. TC2016.

Schwab, M., Ratschbacher, L., Siebel, W., McWilliams, M. O., Minaev, V., Lutkov, V., Chen, F., Stanek, K., Nelson, B., Frisch, W., and Wooden, J. L., 2004, Assembly of the Pamirs; Age and Origin of Magmatic Belts from the Southern Tien Shan to the Southern Pamirs and Their Relation to Tibet: Tectonics, v. 23, no. 4, p. TC4002.

Sippl, C., Schurr, B., Tympel, J., Angiboust, S., Mechie, J., Yuan, X., Schneider, F., Sobolev, S., Ratschbacher, L., and Haberland, C., 2013, Deep Burial of Asian Continental Crust beneath the Pamir Imaged with Local Earthquake Tomography: Earth and Planetary Science Letters, v. 384, p. 165-177.

Sobel, E. R., Chen, J., Schoenbohm, L. M., Thiede, R., Stockli, D. F., Sudo, M., and Strecker, M. R., 2013, Oceanic-Style Subduction Controls Late Cenozoic Deformation of the Northern Pamir Orogen: Earth and Planetary Science Letters, v. 363, p. 204-218.

Stübner, K., Ratschbacher, L., Rutte, D., Stanek, K., Minaev, V., Wiesinger, M., and Gloaguen, R., 2013, The Giant Shakhdara Migmatitic Gneiss Dome, Pamir, India-Asia Collision Zone: 1. Geometry and Kinematics: Tectonics, v. 32, no. 4, p. 948-979.

Tapponnier, P., Mattauer, M., Proust, F., and Cassaigneau, C., 1981, Mesozoic Ophiolites, Sutures, and Arge-Scale Tectonic Movements in Afghanistan: Earth and Planetary Science Letters, v. 52, no. 2, p. 355-371.

Thomas, J. C., Chauvin, A., Gapais, D., Bazhenov, M., Perroud, H., Cobbold, P., and Burtman, V., 1994, Paleomagnetic Evidence for Cenozoic Block Rotations in the Tadjik Depression (Central Asia): Journal of Geophysical Research: Solid Earth (1978–2012), v. 99, no. B8, p. 15141-15160.

van Hinsbergen, D. J., Lippert, P. C., Dupont-Nivet, G., McQuarrie, N., Doubrovine, P. V., Spakman, W., and Torsvik, T. H., 2012, Greater India Basin Hypothesis and a Two-Stage Cenozoic Collision between India and Asia: Proceedings of the National Academy of Sciences, v. 109, no. 20, p. 7659-7664.

Yin, A., and Harrison, T. M., 2000, Geologic Evolution of the Himalayan-Tibetan Orogen: Annual Review of Earth and Planetary Sciences, v. 28, p. 211-280.

Yushin, I. P., Sass, M. E., Karapetov, S. S., Altukhov, S. M., Teplov, I. C., Raeakov, C. R., Harkov, S. I., and Davidchenko, A. G., 1964, J-43-Xxi,Xxii,Xxvii,Xxviii: Russian Geoogical Research Institute.

Zanchi, A., Poli, S., Fumagalli, P., and Gaetani, M., 2000, Mantle Exhumation Along the Tirich Mir Fault Zone, Nw Pakistan: Pre-Mid-Cretaceous Accretion of the

Karakoram Terrane to the Asian Margin: Geological Society, London, Special Publications, v. 170, no. 1, p. 237-252.
Zanchi, A., and Gaetani, M., 2011, The Geology of the Karakoram Range, Pakistan: The New 1: 100,000 Geological Map of Central-Western Karakoram: Italian Journal of Geosciences, v. 130, no. 2, p. 161-262.
Zhu, B., Kidd, W. S., Rowley, D. B., Currie, B. S., and Shafique, N., 2005, Age of Initiation of the India-Asia Collision in the East-Central Himalaya: The Journal of Geology, v. 113, no. 3, p. 265-285.